Data-driven Discrete Well Affinity(DiWA) Model for Production Forecast

Mahdi Asadiesfahani

TU Delft

Data-driven Discrete Well Affinity(DiWA) Model for Production Forecast

Optimization Performance and Model Enhancement

by

Mahdi Asadiesfahani

To obtain the degree of Master of Science

at the Delft University of Technology,

To be defended publicly on Friday October 29, 2021 at 10:00 AM.

Student number:	5139821	
Project duration:	September 1, 2020 – October 29, 2021	
Thesis committee:	Dr. Denis Voskov	TU Delft, supervisor
	Dr. Ali Fadili	Shell Global Solution International B.V.
	Dr. Jeroen Groenenboom	Shell Global Solution International B.V.
	Dr. Hemmo Abels	TU Delft, Assistant Prof.
	Xiaoming Tian,	TU Delft, PhD Candidate

An electronic version of this thesis is available at http://repository.tudelft.nl/.

TU Delft

Preface

The trend of scientific studies in the world of reservoir engineering is inclined to simulation enhancement and optimization. The Data-driven models are the state-of-the-art low-resolution subsurface proxy models, which aim to simulate the dynamic behaviour of reservoir with significantly lower computational cost and acceptable accuracy. In this research, several aspects of the data-driven model are assessed to produce a more reliable framework that enables handling complex physics and heterogeneity.

My master thesis is conducted at *Civil Engineering and Geoscience* department at *Delft University of Technology* under the supervision of **Dr. Denis Voskov**. I thoroughly appreciate his brilliant knowledge in reservoir engineering and computational mathematics, which helped me immensely in my thesis. It is worth mentioning that the main framework of the Data-driven Discrete Well Affinity (DiWA) model is constructed by a TUDelft PhD candidate, **Xiaoming Tian**, whom I am grateful for his guidelines and contributions towards my coding skills and debugging.

This study benefits the opportunity to be validated by a real-life set of field data of an oil reservoir. In this regard, I would acknowledge my industrial supervisors, **Dr. Jeroen Groenenboom** and **Dr. Ali Fadili** who have contributed to my thesis with their professional guidelines during a graduation internship at *Shell Global Solution International B.V.*. Besides, I would like to thank Shell for providing me the opportunity to work with its facilities and data sets in a professional environment during my internship.

Finally, I would thank all the persons supporting me, both mentally and financially, including my parents, *Mehrdad* and *Shahrbanoo*, my sister *Ayda*, and my friends. I wish all the best for them in their life and may God bless everyone.

You can follow me in social media if you want to know more about my subject and interest.

Mahdi Asadiesfahani
Delft, October 2021

Acknowledgement

This dissertation has benefited several powerful resources to be completed. Therefore, I would acknowledge people and organizations supporting these resources.

First of all, I would appreciate the DARTS team who has developed the state-of-the-art Delft Advanced Reservoir Terra Simulator (DARTS) [9] which has increased the computational power of the DiWA model to a large extend. The main computational body of this research is developed with *Python* coding language utilizing various packages and libraries namely *SciPy* [26], *NumPy* [11] and *Pandas* [20], which contributed in optimization, numerical mathematics, and data analysis respectively. The discretization and the visualization of the outcomes of the project are performed by the *Gmsh* [8] and *ParaView* [19] software tools, which are professional packages for creating unstructured grid mesh and visualizing large data. In addition to coding tools and libraries, a part of this project was modelled using geo-modelling tool; *Petrel* [24], which is compelling software for reservoir modelling and geosciences. In this regard, I acknowledge *Shell Global Solution International B.V.* and *TU Delft* for providing licenses for the software.

Abstract

Evaluating an adequate computer model representing the characteristics of a subsurface reservoir is of great importance in the oil and gas industry. With recent data acquisition developments, high-resolution geological models can be generated for the subsurface reservoirs; however, uncertainties of geological data and too many details in the model have brought up remarkable limitations for application of high-fidelity geo-models in reservoir management. To generate efficient low-resolution models, which are relatively representative of the reservoir dynamic behaviour, data-driven models are proposed. The data-driven models are trained principally based on the production history of the reservoir with primary knowledge of structural information. The Data-driven Discrete Well Affinity (DiWA) model is designed to generate efficient proxy models that require basic geological information and full production history of the reservoir. Since it benefits the computational power of the Delft Advanced Terra Simulator (DARTS) and adjoint gradient-based optimization, the DiWA model has become an efficient framework in terms of accuracy and computational costs. This research shows that the DiWA model can relatively reconstruct the reference reservoir parameters out of an ensemble of priors, and the final results can be improved utilizing closer prior knowledge to the true response. Additionally, it is demonstrated that the performance of the DiWA model in a complex, realistic oil field can be enhanced using a comprehensive objective function, applying appropriate well controls, understanding the underlying driving mechanisms, using sufficient degrees of freedom, and applying consistent boundary conditions.

List of Tables

List of Figures

Contents

1 Introduction

In the Oil and Energy industry, many methods and techniques attempt to simulate the complex dynamic behaviour of fluid flow in subsurface applications. Although several mathematical models have already been developed to perform simulations over fluid flow inside a reservoir within a reasonable accuracy and efficiency range, recent studies endeavour to establish models with higher computational capacities.

Even though there are possibilities to develop high-resolution geological models, the model resolution will exceed a few million grid cells, which brings out an expensive computational cost when performing dynamic simulation at such a high resolution. In addition to high computational cost, geological information always encompasses various uncertainties due to measurement errors, which has still put the reliability of high-resolution geo-models under debate. Another issue inherent in high-resolution geo-models would be the fact that in reservoir management applications such as history matching or production optimization, a considerable number of simulation runs is required. This is not computationally feasible to perform using high-fidelity models.

To overcome these issues, numerous reduction solutions are proposed. However, the technique of evaluating simplified models with adequate representation of the realistic response might be the most traditional proposal among the others. Techniques such as *upscaling*, *multi-scale models*, *streamlines* , and various *data-driven models* are more prevailing than other methods which attempt to simplify the high-fidelity reservoir models. Upscaling is the method of coarsening the resolution of the fine-scale model to decrease the number of grid blocks and, accordingly, the computational cost. The properties in the upscaling method are assigned effectively to coarser blocks to perform a similar response as high-fidelity models [12]. When it comes to more complex physics or dynamics, upscaling methods can not estimate the reservoir flow response accurately; thus, multi-scale methods were proposed. The multi-scale methods attempt to capture the full original model resolution and define large-scale solutions effectively without resolving coarse-scale in details [16, 13]. The streamline method is a technique of evaluating fluid transport paths along the streamlines by having grid pressure values calculated effectively beforehand, which is recently capable of solving three-phase large-size reservoirs [1].

All the methods as mentioned earlier require the high-resolution geological model as a basis to perform simplification. Moreover, the resulting coarser model does not guarantee a similar production history since it is constructed only based on geological reservoir parameters and still requires calibration. To reduce the dependency of the course model on the geological data, *data-driven* proxy models can be used. In principle, a data-driven model is a low-resolution reservoir model in which the reservoir parameters are regressed using production history to deliver a similar reservoir response.

There are several data-driven approaches designed to create low-resolution proxy models for the reservoir:

- **Non-Stationary Data-driven Models**: The primary attempts to build data-driven models are conducted when the stationary methods for interpolating geological properties between wells become inefficient. Consequently, to overcome the issues inherent in the geostatistics interpolation methods, an inter-well connectivity model was created to consider the well production response in the interpolation. Janaen et al. l [14] have introduced a non-stationary data-driven model for inter-well connectivity networks. In this approach, first, the missed data of the wells are interpolated using a crossed correlation between sampled and unsampled locations. Second, the searching neighbourhood is defined to apply the inter-well model on that. Considering the mentioned assumptions, an experimental variogram for the intermediate properties can be developed to interpolate geological properties between wells.

- **Capacitance-Resistance Model**: The methodology of CRM is attempting to quantify the connectivity between wells using only production and injection rates. The flow barriers and permeability trends are recognized by investigating the linear regression procedure with the diffusivity filter. With the hands of *Multivariate Linear Regression (MLR)* method, the issue inherent in the unbalanced flooding of the injectors is solved in this method. Furthermore, it is proved that CRM data-driven framework can project the oil production rate with only available injection rates [2]. The fluctuation in the production data due to noises and measurement errors has led studies to develop a more completed CRM method to deal with this issue. Yousef et al. [28] proposed a CRM model including compressibility (capacitance) as well as resistive (transmissibility) effects to cover unsteady-state (i.e., not only including transmissibility) inter-well communication.

- **Interwell Numerical Simulation Model (INSM)**: The concept of the INSM model is based on the fact that the connectivity between wells can be modelled assuming a control unit between wells that are navigating the flow. According to [29], each control unit is governed by transmissibility and control pore volume factor. The flow paths and barriers can be modelled by solving the material balance between each pair of wells. The new INSM approach has some advantages over the previous correlations for inter-well connectivity; (1) the reservoir parameters are approximated through a history matching process; thus, the model is capable of dealing with fluctuations in rates caused by shutting or switching wells; (2) the new INSM approach can model separate phase fluid production; (3) field waterflood optimization can be applied on INSM with relatively less computational effort.

- **Reduced-Order Model (ROM)**: Recently, since the ROM [7, 3] method reduces the time of forwarding simulation significantly, it is extensively used in many other optimization applications outside reservoir engineering. The basis of the ROM model is the assumption that the forward simulation response can be achieved with many fewer degrees of freedom (i.e., the model parameters such as transmissibility and well index to be trained). In reservoir engineering applications, e.g., [6], the ROM is combined with the *Proper Orthogonal Decomposition* method in which, in each forward run, solution snapshots are stored, and eigen-decomposition is performed on the resulting matrix. This methodology proves that the simulation time has reduced significantly, and the proxy model could generate the high-fidelity model with an acceptable tolerance.

In this framework, we utilize and further extend *Discrete Well Affinity (DiWA)* model [25]. The prior guess encompasses the structure of the reservoir, an approximation of petrophysical properties, and initial reservoir condition. The defined prior proxy model is then trained with the production history by an optimizer (e.g., *Sequential Least-Square Programming (SQLP)* method used in this research) to adjust model parameters so that the production history is satisfied. The solver engine used in this subject is the *Delft Advanced Terra Simulator (DARTS)* which benefits the power of Operation-Based Linearization technique [27] in solving complicated physics.

The noticeable advantage of the DiWA model is that the model is not fully dependent on the production data. Considering a prior initial geological guess from the reference model as a starting point, the optimizer will be constrained to a realistic range of parameters next to the production data. Taking the advantage of DARTS simulator, the *adjoint-based gradient* can be utilized for the training process to increase the speed of convergence and reduce the computational cost to a large extend [25]. Providing a reasonable prior guess for the training process, the resulting proxy model performs more accurately

than one based on a random one. Despite the traditional history matching methods in reservoir management applications, which the original uncertain geo-model had to run several times, the DiWA model can be utilized in field optimization and history matching operations with a relatively faster calibration time.

1.1. Thesis Objectives

Similar to the other history matching methods, which aim to produce a model that satisfies the production data, the main intention of the DiWA model is to reconstruct an efficient low-resolution reservoir model for the underlying geological properties and fluid physics. Constructing an efficient proxy model requires a broad investigation into the influence of the input prior knowledge and the optimization settings on the training performance. The research question is ”To what extent can the initial prior knowledge affect the optimization performance both in synthetic and field cases?” The research question is too broad to be answered at once; thus, some sub-questions are designed to cover the main question:

- **Reconstruction of Reservoir Parameters**: Is the optimizer capable of reconstructing the reference reservoir parameter after the training? If yes, is the solution unique? In the case of non-uniqueness, what considerations must be made to constrain the problem to the realistic parameters?
- **Optimization Error and Iteration**: How will the optimizer perform with perturbed initial guesses around the original reference model? Does a more perturbed initial guess increase the error and the computational cost (i.e., number of optimization iteration)?
- **Real-life Field data**: What additional considerations for the prior knowledge and the optimization settings have to be made when dealing with real field data? How should the DiWA methodology be adapted in the case of insufficient control variables (i.e., when consistent BHP measurements are missing)?

1.2. Workflow and Research Procedure

The research workflow is designed to start with simple synthetic models attempts to analyze the flexibility of the DiWA model with various optimization settings and initial guesses. Afterwards, the framework is examined with real data to analyze the framework’s capability in a realistic field situation. Table 1.1 summarizes the thesis objectives and workflow in a total of five stages.

	Approach	Objective
Stage 1	Synthetic Reference model	Create true production response and reference geological model to examine performance of the optimizer based on that.
Stage 2	Structured Proxy model	Investigate the ability of the training framework to reconstruct the reference model. Additionally, examine the sensitivity of the optimizer to various initial guesses for the proxy model.
Stage 3	Field data Pre-processing	Analyzing the filed data to understand the underlying physics and the production strategy of the oil reservoir
Stage 4	Unstructured Proxy model	Create an adequate training framework with unstructured discretization method to evaluate a PDDM model for the field data
Stage 5	Field Proxy model Enhancement	Investigate the possible solutions to improve the performance of the proxy model created for the oil field data.

Figure 1.1: Thesis objectives and workflow in five stages. The first column represents the title of the scientific methodology used in each stage. The second Column describes the objective of the corresponding approach.

2

Methodology

In this chapter, a comprehensive description of the mathematical formulation is provided based on basis of physical principles which governs formulations for flow and transport in porous media. The content is supported with an explanation of the theory behind the state-to-the-art advanced *Operation-based linearization technique (OBL)*. In the second part, the principle of the *History Matching* and the *Inverse Problem solution* is broadly analyzed. Finally, the formulation of an unstructured grid discretization and the implementation of control variables (modifiers) are pointed out.

2.1. Mathematical Formulations for Fluid Flow in Porous Media

The mass conservation equation for fluid flow in a porous media is given by equation 2.1 for n_c number of components. All the variables used in equation 2.1 are defined as a function of the spatial coordinate of ξ and the physical state of ω

$$\frac{\partial}{\partial x}(\phi \sum_{j=1}^{n_p} x_{cj}\rho_j S_j) + \nabla \sum_{j=1}^{n_p} x_{cj}\rho_j v_j + \sum_{j=1}^{n_p} x_{cj}\rho_j q_j = 0. \tag{2.1}$$

In equation 2.1, $\phi(\xi)$ is the porosity, $x_{cj}(\omega)$ is the molar fraction of component c and phase j, $s_j(\omega)$ is the saturation of phase j, $\rho_j(\omega)$ is the phase density, $v_j(\xi,\omega)$ is the *Darcy Velocity* of phase j, and $q(\xi,\omega)$ is the phase rate in the borehole (i.e. source term).

The *Darcy Velocity* is calculated as follow

$$v_j = -(k\frac{k_{rj}}{\mu_j}(\nabla\Phi_j)), \tag{2.2}$$

where k is the absolute permeability of rock, k_{rj} is the relative permeability of the phase j, μ_j is the viscosity of phase j and Φ is the phase potential defined as $\nabla p_j - \lambda_j \nabla d$ in which d is the vector of depth (positive downwards), λ is the gravity term and p_j is the phase pressure.

Using backward Euler approximation in time and finite-volume discritization for mass conservation equation, equation 2.1 can be restated as

$$V\left((\phi \sum_j x_{cj}\rho_j S_j)^{n+1} + (\phi \sum_j x_{cj}\rho_j S_j)^n\right) - \Delta t \sum_{l\in L}\left(\sum_j x_{cj}^l \rho_j^l T_j^l \Delta\psi^l\right) + \Delta t \sum_j \rho_j x_{cj} q_j = 0. \tag{2.3}$$

2.1.1. Operation-Based Linearization (OBL) Technique

In principle, the OBL linearization technique aims to represent the discretized form of conservation equation (2.3) in an algebraic form in which parameters that are dependent on spacial and physical properties are separated in different operators (represented as α and β). Equations 2.5 to 2.9 are the operator form of conservation equation in which c_r is the rock compressibility factor, u is the control vector, and T^{ab} is the geometric part of transmissibility factor between grid blocks a and b:

$$R_c(\xi,\omega,u) = a(\xi)(\alpha_c(\omega) - \alpha_c(\omega_n)) - \sum_l \beta_c^l(\omega) b^l(\xi,\omega) + \theta_c(\xi,\omega,u) = 0, \tag{2.4}$$

$$\alpha_c(\omega) = \big(1 + c_r(p - p_{ref})\big) \sum_j x_{cj}\rho_j S_j, \tag{2.5}$$

$$\alpha(\xi) = V(\xi)\phi_0(\xi), \tag{2.6}$$

$$\beta_c(\omega) = \sum_p x_{cj}(k_{rj}/\mu_j)\rho_j, \tag{2.7}$$

$$b(\xi,\omega) = \Delta t T^{ab}(\xi)(p^b - p^a), \tag{2.8}$$

$$\theta_c(\xi,\omega,u) = \Delta t \sum_j \rho_j x_{cj} q_j(\xi,\omega,u). \tag{2.9}$$

To solve the system of non-linear equations 2.4, a linearization method is required first. In reservoir simulation, the pervasive approach is based on the *Newton-Raphson* method. The advanced *Newton-Raphson* method is an iterative solver that can resolve the residual form of equation 2.3 in each iteration till it satisfies the convergence criteria. Equation 2.10 describes the Newton-Raphson method

$$J(\omega^k)(\omega^{k+1} - \omega^k) = -R(\omega^k), \tag{2.10}$$

where j is the Jacobian matrix of physical variables ω at non-linear iteration k, and R is the residual form of equation 2.3.

The typical linearization approach requires an assembly of residual form of the conservation law and the corresponding numerical approximation of the Jacobian. This method may need interpolations for PVT and relative permeability tables or expensive computational effort on evaluating these properties out of non-linear EoS-based equations. On the other hand, the OBL technique is based on a sophisticated combination of various non-linear properties and relations which simplifies the representation of the non-linear operators in the parameter-space of a simulation problem. The significant advantage of the OBL technique comparing to other conventional simulators is that it reduces the computational cost of solving the non-linear system by separating spatial and physical operators. Despite the conventional simulators, which solve conservation equations only based on time and spatial discretization, the differentiation procedure in the OBL is conducted over all non-linear physical parameters with a direct interpolation. Therefore, utilizing such a technique in a history matching problem will enhance the forward simulation results and reduce the convergence iteration took by the optimizer to a large extend [27].

2.2. History Matching and Inverse Problem

A history matching problem is considered an inverse problem in which the reservoir model parameters are evaluated to satisfy the reservoir observed behaviour. In principle, a history matching problem is ill-posed; this means that very different combinations of the reservoir parameters (such as transmissibility, well indexes, and non-linear parameters) can lead to a reasonable misfit between model response and observed data. This is an indication of the non-uniqueness of the solution to a history matching problem. A history matching problem aims to minimize the misfit between the observed data and the

model response. Usually, misfit objective function represents the difference between the physical status of the reservoir (pressure distribution and the phase saturation) and the simulated results [5, 12].

The inherent risk with this type of objective function is that the pressure and the saturation data are only found in the well locations and are regionally limited. A further shortcoming of the physical status objective function would be the considerable uncertainty created by interpolating pressure and saturation values between wells. To tackle this issue, the misfit between the fluid production history of the target reservoir and the model fluid rate response can be used as an objective function in the history matching problem. The reason behind is that the production history is available in almost all fields, and it is continuously recorded through the lifetime of the reservoir [22].

In an inverse problem, the transport equation is a function of the state variables that express the reservoir condition in terms of pressure and saturation and the model parameters that control the fluid flow in the transport equation. In this study, the model parameters are referred to as *Control Variables*, and the generalized governing equations for isothermal oil-water flow in porous media (state equation) is expressed as follow:

$$g(x,u) = 0, \quad x(t_0) = x_0, \quad t \in [t_0, t_f], \tag{2.11}$$

where t is time, x is the state variable (phase pressure and saturation), and u is the vector of control variables (reservoir transmissibility, well indexes and Brooks-Corey or other parameters for relative permeabilities).The first expression in equation 2.11 represents the partial differential equation for mass balance in porous media and the second one indicates the initial condition of the model.

The objective function in a history matching problem is commonly defined as a least-square data misfit:

$$J(u) = \frac{1}{2}\left[q(u) - q^{obs}\right]^T C_D^{-1}\left[q(u) - q^{obs}\right] + R, \tag{2.12}$$

where J is the objective function, $q(u)$ is the vector of production or injection rates given by the proxy model (model response), q^{obs} is the observed rates or high-fidelity model response (named as "true response"), C_D is the measurement error, and R is the regularization term which can be added to the objective function in case of model reparametrization [5].

The aim of history matching is to minimize the objective function ($J(u)$) with certain constraint of $d(u)$ as it is represented by equation below:

$$minJ(u), \quad d(u) \leq 0. \tag{2.13}$$

In this framework, the objective function is defined in discrete format in time for all wells and separated phases assuming no regularization term as follow:

$$\sum_{t=1}^{n_{ts}} \sum_{w=1}^{n_w} \left(\sum_{j=1}^{n_p} q_{t,w,j} - \sum_{j=1}^{n_p} Q_{t,w,j} \right)^2, \tag{2.14}$$

where $q_{t,w,j}$ and $Q_{t,w,j}$ are the model and the true response of the reporting time of t for well w and phase j respectively.

2.2.1. Adjoint Gradients for Optimization

In a gradients-based history matching, the misfit objective function should be minimized by an optimizer. To achieve such a minimum, the gradient of the objective function related to the control variables is required as an iterative feed to the optimizer in every timestep. One of the issues inherent in the gradient calculation is that the relationship between the state and the control variables are related through a preservation of partial differential equation (i.e., equation 2.11), and it makes the gradient evaluation procedure complicated to a large extent. Therefore, the method calculating the gradient of the objective function is of great importance in terms of both accuracy and efficiency [5, 15]. As a simple solution, a numerical gradients can be evaluated with acceptable accuracy; however, the

computational cost for the numerical derivations is significantly large as it requires a forward simulation in each evaluation of the partial derivatives in the gradient at each timestep. A more efficient method to compute gradients is the *adjoint gradient* technique, which is significantly faster than the numerical gradients method.

One of the most efficient method to calculate the adjoint gradient of the objective function is based on the *Optimal Theory* derived by Stengel [21]. Since the dependency of the changes of the objective function j to the change of the control variable u is implicit, a *Lagrangian* multiplier λ is used to derive a modified version of the objective function $\bar{J}$ that addresses the same extrema with the original objective function J as follows:

$$\bar{J}(\omega, u, \lambda) = j(\omega, u) + \lambda^T g(\omega, u), \tag{2.15}$$

where the λ^T is the transpose of the Lagrangian multiplier. By evaluation the Lagrangian formulation, the space of optimization with ω and λ is increased and the non-linear constraint on g is ignored. The optimum solution of the equation 2.15 with respect to ω, u and λ occurs on the boundary of the feasibility region or at the stationary point. Equations 2.16, 2.17 and 2.18 are the variation of the Lagrangian equation 2.16 with respect to λ, ω and u.

$$\overline{J_\lambda} = j(\omega, u) = 0, \tag{2.16}$$

$$\overline{J_\omega} = \lambda_{g\omega}^T(\omega, u) + J_\omega(\omega, u) = 0, \tag{2.17}$$

$$\overline{J_u} = \lambda_{gu}^T(\omega, u) + J_u(\omega, u) = 0. \tag{2.18}$$

As it is clear from equation 2.16, the variation of the Lagrangian with respect to λ is the state equation of the reservoir. Accordingly, equations 2.17 and 2.18 are the *adjoint* and the *optimization* equations respectively. Equation 2.16 is already satisfied through the non-linear iterative solver and the Lagrangian multiplier is evaluated from equation 2.16 and then the solution to the optimization problem is obtained from equation 2.18. The accuracy and the performance of the gradient-based optimization for both adjoint and numerical method are studied to stay at physical range of the problem by imposing a large penalty term for non-physical region.

2.2.2. Optimization Bounds and Constraints

In the inverse problem, the optimizer tempts to optimize the objective function with a given initial guess of the model parameters. Depending on the optimizer, the physical value of the control variables fed to the optimizer must be in a reasonable range and possesses a sensible value. For instance, the *Sequential Quadratic Programming (SQP)* nonlinear optimizer used in this study will perform more efficient if the control variables are normalized to values between 0 and 1.

it is crucial that the value of the initial guess drops in the optimizations bounds, otherwise the solution is not reliable and optimizations collapses. It can be suggested to use a wide range for bounds to reduce uncertainty of dropping out of the bounds, however, this can increase the computational time significantly and make the optimizer to converge to another local optimum. To determine an efficient optimization bounds, it is proposed that the bounds can be evaluated with initial approximation of the magnitude of the control variables for the initial guess and extend it by 1.5 - 2 times.

Here is the optimization bounds for Brooks-Corey parameters used in this study

$$\mathbf{u}_n = S_{or}, Swc, n_o, n_w, \frac{k_{rw}^e \rho_w}{\mu_w}, \frac{k_{ro}^e \rho_o}{\mu_o} \tag{2.19}$$

$$\mathbf{u}_{n,min} = \{0.0, 0.0, 10^{-5}, 10^{-5}, 100, 10\}, \tag{2.20}$$

$$\mathbf{u}_{n,max} = \{0.49, 0.49, 6, 6, 2000, 2000\}, \tag{2.21}$$

2.3. Unstructured Discretization

In the numerical reservoir simulation and production optimization, the process of discretization and the way that the reservoir is getting meshed is inevitably important. In principle, the system of the grid cells constructs the basis of the discretization process and in this study the unstructured partitioning and finite-volume democratization is used to build the data-driven proxy model [17]. The associated transmissibility and connections between unstructured grids is then represented by the resulted connectivity graph based on the mesh shown on figure 2.1.

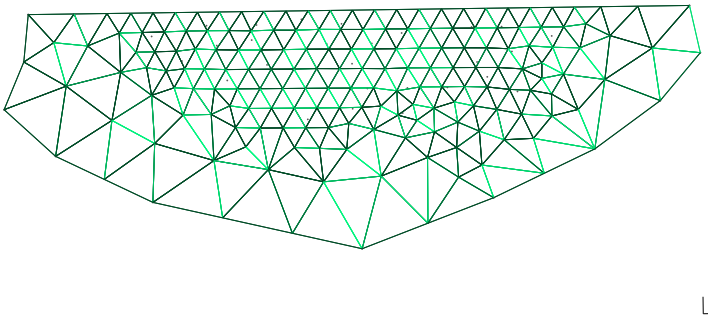

Figure 2.1: Data-driven proxy model grid cell system discritized in unstructured grid format.

In order to build a mesh for a target reservoir, the coordinates of the boundaries, well location, and the whole geometry of the reservoir need to be defined. If high-fidelity model exist, this data is usually given based on Cartesian grid with active and inactive cells which forms the particular shape of the reservoir. To define an efficient resolution for the reservoir, a systematic methodology to create finite-volume grid cells has been developed using *Gmsh* package [10].

There can be two possible ways creating mesh grids using *Gmsh*:

- **Using the *ECLIPSE* input data file**. The Eclipse files including grid cells sizes and depths for high-fidelity model have been red by a Python based code as well as the *ACTNUM* file which determines the active and inactive cells to form the general shape of the reservoir. The total number of grid cells are defined based on resolution for each points. The average coordinates of the first top layer of the reservoir have been used to create the boundaries of the reservoir as an input to *Gmsh* package. All the well coordinates are exactly as the real coordinates; however, some points on the boundary has been corrected to fit the real shape.

- **Building the mesh from the geomodel**. Building mesh system from reservoir geomodel requires the coordinates of points defined at the boundary of the reservoir contour, then the overall shape of the reservoir is constructed with extrusion over the surface created with points on the boundary.

Comparing mesh constructed from geomodel and ECLIPSE data file, the mesh system created based on the ACTNUM file is more precise since the ECLIPSE data file includes active cells in all the layers in three dimensions which leads to more accurate reservoir geometry. The process of 3D meshing for the first top layer of the reservoir is conducted with *HXT* meshing algorithm which reduces the number of tetrahedral in meshing process and uses prisms instead. The mesh sizes around the wells are set to be approximately 10 times lower than other locations in the mesh grid system to increase the accuracy and precision of the solution around each well. The method ‘Distance’ and ‘Threshold’ of *Gmsh* package have been utilized to increase number of meshes around the well by a predefined radius.

2.4. Model Modifiers

The term *Model Modifier* refers to model parameters which are set to be optimized during the training period. Modifiers can be well controls or a reservoir parameter such as well index or transmissibility. In this study, the model modifiers used for training are the reservoir transmissibilities, well indexes, and relative-permeability model parameter (e.g. Brooks-Corey correlation or Stone model parameters for relative permeability).

2.4.1. Fluid modifiers

For estimating fluid-rock properties such as relative permeability, conventional correlations are used. These correlations are non-linear with respect to flow rate (i.e. the Darcy's law). The major issue inherent the fluid modifiers is the complexity they add to the main solution loop of the reservoir transport equation. In addition, the gradient evaluation process will significantly affected by non-linear behaviour of some modifiers.

The Brooks-Corey correlation (or simply the Corey correlation) [4] for determining phase relative permeability for a multi-phase fluid flow in porous media is widely applied in the reservoir simulations. The theory utilizes the effective water saturation S_w^* and endpoint relative permeability k_r^e for each phases to estimate the relative permeability versus water saturation as follow

$$k_{ro} = k_{ro}^e (1 - S_w^*)^{n_o}, \tag{2.22}$$

$$k_{rw} = k_{rw}^e (S_w^*)^{n_w}, \tag{2.23}$$

$$S_w^* = \frac{S_w - S_{wc}}{1 - S_{wc} - S_{or}}. \tag{2.24}$$

2.4.2. Reservoir Modifiers

In reservoir discritization, the connection between each grid cell is characterized by a spatial connectivity mesh system. It encompasses the connectivity and spatial relationship between grid cells with their corresponding transmissibility at their interface. For a general unstructured grid system, the transmissibility [18] is defined as

$$\Gamma_{ij} = \frac{\alpha_i \alpha_j}{\sum_n \alpha_n}, \alpha_i = \frac{A k_i}{D_i}, \tag{2.25}$$

where A is the cross area of the interface, D is the distance of the pressure node to the interface along the line connecting the two pressure nodes, and k_i is the permeability of the cell i.

2.4.3. Well Modifiers

There are plenty of well models estimating the well connectivity to the cell in which well is located. The well transmissibility (or commonly known as the *Well Index*) is a function of physical properties as well as the geometric shape of the grid cell which is linear with respect to fluid flow rate as follow:

$$q_i^w = \frac{WI_i}{\mu}(P_i - P_i^w). \tag{2.26}$$

Perhaps the most practical well model to estimate the well index is the Peaceman equation [23] which includes a equivalent cell radius calculated from geometry of the cell and permeabilities in y and x directions

$$WI_i = \frac{2\pi\delta z\sqrt{k_x k_y}}{lnr_o/r_w + S}, \tag{2.27}$$

$$r_o = 0.28\frac{\left[(k_y/k_x)^{1/2}\Delta x^2 + (k_x/k_y)^{1/2}\Delta y^2\right]^{1/2}}{(k_y/k_x)^{1/4} + (k_x/k_y)^{1/4}}. \tag{2.28}$$

2.5. Model Upscaling Methods

In terms of comparison or using more precise initial guess for the training process, two types of geological upscaling methods are used to evaluate the control variables in lower resolution from the true fine-scale model which are the *volume-weighted averaging* and *flow-based upscaling*.

2.5.1. Global Flow-based Upscaling

The global flow-based upscaling is an efficient conventionally used method to evaluate the course model's transmissibility and Well Indexes by solving the single-phase Darcy's law in the course scale as follow:

$$(q^C)_{i+\frac{1}{2},j} = (T^C_{i+\frac{1}{2}}) \left(P^C_{i,j} - P^C_{i+1,j}\right), \tag{2.29}$$

where $(q^C)_{i-\frac{1}{2},j}$ is the flow rate at the course interface $i+\frac{1}{2}$ which is simply the summation of the rates at the corresponding fine-scale interface, $T^C_{i+\frac{1}{2}}$ is the upscaled transmissibility to be evaluated by this equation and $P^C_{i,j}$ is the pressure at the cell center of $i+1, j$ which is simply an arithmetic average of the pressures in the fine-scale. With the same methodology, the well indexes in the course scale can be easily evaluated utilizing well bottom hole pressure and course block pressure (i.e the pressure of the course-scale block which is evaluated with arithmetic averaging) as follow

$$WI_{course} = \frac{q}{P^C - P_b hp}. \tag{2.30}$$

2.5.2. Volume-weighted Property Averaging

The Volume weighted averaging is a simple geometric method used to upscale geological properties from the fine-scale to the course-scale grids. This method is only used for the porosity upscaling in structured grid and porosity projection to the unstructured grid. It is defined as follow:

$$G_C = \frac{\sum_{i=1}^{n} V_i P_i}{\sum_{i=1}^{n} V_i}. \tag{2.31}$$

2.6. Data-driven framework

In this framework, there are two major approaches to investigate the data-driven models: *Deterministic* and *Stochastic*. In the deterministic approach, the initial guess of the optimizer is built straightly out of geological data with the hands of upscaling techniques to project petrophysical properties such as porosity and permeability from high-fidelity to the proxy model. On the other hand, in the stochastic approach, the ensemble of realizations from petrophysical properties are created and fed to the optimizer. The noticeable point in creating various realizations is that they all possess exact stochastic settings (i.e. they are either constrained to the wells or have an equal mean and standard deviation) and modelled with the same property modelling algorithm. Figures 2.2 and 2.3 illustrate schematics explaining deterministic and stochastic data-driven approaches step-wise.

In order to build an efficient DiWA model, an extensive framework containing three main steps is designed in this study. The initial stage encompasses the pre-processing of the raw data, and it ultimately depends on the availability and the type of data provided. Following the pre-processing step is the geological definition of the proxy model's prior knowledge, which can be evaluated from well logs or high-fidelity geo-model. The last step is the training process in which the objective function is optimized, and control variables (or modifiers) are evaluated to satisfy the convergence criteria.

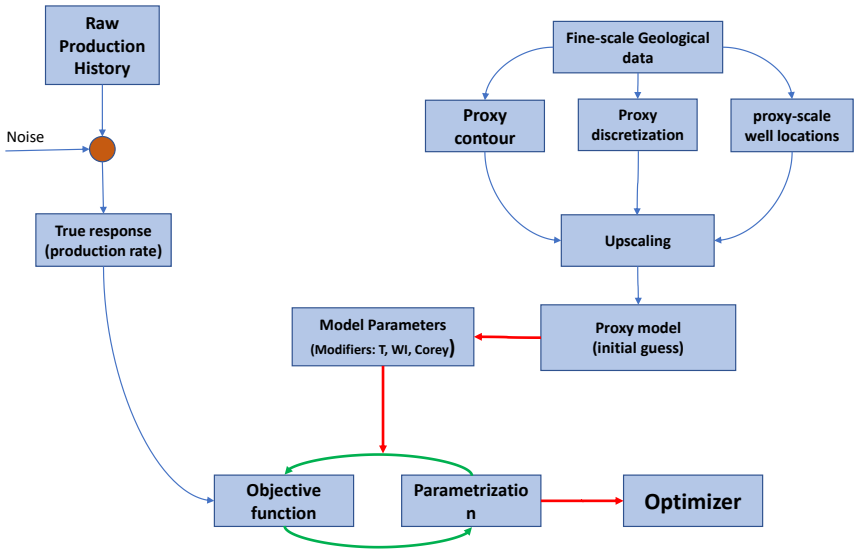

Figure 2.2: Deterministic Data-driven approach framework; It is shown by this schematic that the production and geological data are taken as raw information and then processed separately. Then a single upscaled proxy model is evaluated out of petrophysical data. The resulting proxy model is fed to the optimizer with defined modifiers (in this study T: transmissibility, WI: well index, Corey: Brooks-Corey correlations parameters). In the objective function, parametrization might be included to penalize the objective function in the optimization loop to avoid locally convergence

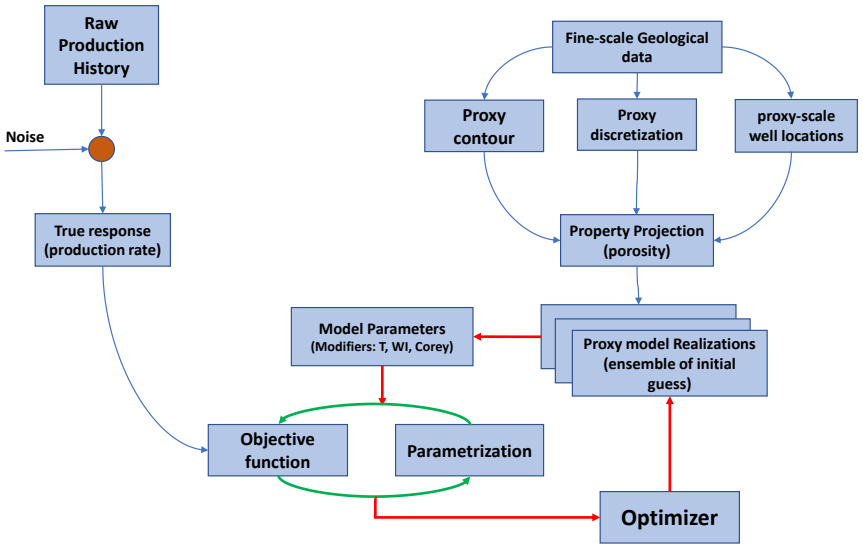

Figure 2.3: Stochastic Data-driven approach framework; It is depicted by this schematic that the production and geological data are taken as raw information and then processed separately. Then the ensemble of realizations are created out of petrophysical data. The resulting proxy model is fed to the optimizer with defined modifiers (in this study T: transmissibility, WI: well index, Corey: Brooks-Corey correlations parameters). In the objective function, parametrization might be included to penalize the objective function in the optimization loop to avoid locally convergence

2.6.1. Data Pre-processing

In a history matching problem, the data set provided plays a crucial role in the optimization performance and the reliability of the results. In principle, all data sets can be categorized into two main groups:

- **Production History**: In the pre-processing stage of production data, some interpolations between well production rates might be required due to measurement noises and discontinuity of the timesteps. The noise accompanies with the production history can be taken into account by introducing the covariance matrix to the objective function (i.e. the C_D term in equation 2.13). The selection of the reporting time step depends on the convergence criteria of the forward simulation of the proxy model in the training process. A larger reporting timestep will make the data smoother and eliminates the outliers in the data.
- **Well Controls**: One of the essential parameters fed to the optimizer as a control on the objective function is the well controls. Wells can be controlled by BHPs or by fluid rates. The DiWA framework can perform with two types of well controls, and the selection of the type of control depends on the availability of the pressure or rate data. In most cases, the BHP data are very rare or not available at all; in this case, the *Heuristic BHP* method can be used to develop BHP data out of rates for the model or apply purely rate control for the wells.
- **Geological Properties**: Geological information can be given both in terms of well logs or high-fidelity geo-models. When well logs are available, a translation of the logs to petrophysical properties is required following an interpolation between the wells to create the property distribution. If the high-fidelity geo-model is provided, a proper property projection method must be selected to transport properties such as porosity from the high-fidelity to the proxy model. Methods such as *Geometric Upscaling* and *Flow-based Upscaling* can be used to project the properties to the proxy model.

2.6.2. Definition of Prior Ensemble

The prior geological knowledge of the proxy model can be obtained in various ways. The prior knowledge contains information about reservoir contour (boundaries), pay zones, the initial estimation of the Standard Total Oil Initial in Place (STIOP), presence and strength of the water drive aquifer, location of the wells and perforations, Net to Gross ratio (to find discontinuities in the reservoir), porosity distribution and the porosity-permeability relationship. If the high-fidelity geo-model is available, the upscaled porosity and permeability model can be used as prior knowledge of the training process; however, in most cases, the high-fidelity geo-model is uncertain or is not available. In such a situation, the prior porosity and permeability can be modelled using well log information and stochastic property modelling methods.

2.6.3. Model Training

The training process is a comprehensive procedure which includes the definition of the proxy model with the prior knowledge of the geological data and the well locations. In addition, fluid-rock dynamic properties, well controls (whether it is BHP or rate control) and simulation convergence limits are set in this stage. They key elements in a successful training procedure are the scaling factor, optimization bounds, degrees of freedom, and the type of the optimizer which has to be set precisely.

The objective function can represent the differences in the production fluid rates, well BHPs, injection rate, and fluid saturation. Depending on the type of objective function used, the values of the well controls have to be set so that the prior proxy response gets closer to the true data. Since the overall geometry and STOIIP of the proxy model and the true model are tuned to be equivalent, the same well control conditions are applied on the proxy model. The proxy model is fed to the optimizer with predefined prior knowledge and well controls similar to the true model (or the reference model). The optimizer can operate with a random or perturbed initial guess of the control variables (or modifiers)

within its physical bounds; however, the initial guess can be obtained from the properties of the proxy model. The problem's solution (i.e. optimized parameters) is obtained after several iterations running many forward simulations. The computational time depends on the size of the Degrees of Freedom (i.e. number of parameters to be optimized), the complexity of the physics, and the type of modifiers used.

3

Synthetic Oil Field

In this chapter, first the method and the theory used to create all the synthetic reference and proxy models are discussed in details. For evaluating a data-driven model, a reference model is created to generate a ”true response”. The structure and the properties of the synthetic two-dimensional reference model is explained followed by a thorough description of the structured proxy model. Afterwards, the results and the analysis of outcomes are demonstrated and discussed in details.

3.1. Synthetic Reference Model

In order to investigate the research question of the impact of various initial guesses on the training performance, a synthetic reference model had to be built to evaluate the true response of the training procedure. The model is constructed in DARTS[1] framework and the properties such as porosity realizations are modeled in Schlumberger Petrel [2] software.

The reference model is a 2D square with the size of 400 by 400 by 10 meters discretized by 108 by 108 by 1 grid cells and consists of two producers and two injectors. The model resolution is set in a way to provide consistency in the well locations as the model is coarsen for building proxy models. The well location consistency is crucial to compare various proxy models with the reference model as the distance between wells may change when creating a proxy model. In order to evaluate the reference model resolution (e.g. 108 in this study), consider a simple 4 by 4 by 1 structured model (as depicted by figure 3.1) which each well is located at the center of grid cells with the coordinates of (0, 0), (0, 3), (3, 0) and, (3, 3). Then each grid is divided by three both in vertical and horizontal directions to increase the resolution and keep the overall size of the model at the same time. In the finer model, the well locations are again at the cell center with the coordinate of (1, 1), (1, 10), (10, 1) and, (10, 10). If the division procedure continues, after two steps (the first step is not considered) the resolution of 108 by 108 is gained.

The properties such as porosity for the reference model are evaluated by the *Property Modeling* feature of Petrel. The entire property distribution is modeled with *Sequential Random Gaussian Distribution* and is constrained to the synthetic well logs. The variogram settings are set to values representing lowest effect of noise in the well data for petrophysical modeling which is the nugget value of 0.0001 and sill value of 1. Number of 1000 realizations are created for the porosity distribution of the reference model to be utilized in stochastic data-driven approach. As for the permeability of the reference model, the Karman-Cozeiny correlation with average grid size of $1E^{-8}$ meter and tortuosity of 180 are used to develop porosity-permeability relationship. Equation 3.1 and figure 3.2 represent the mathematical

[1] Delft Advanced Reservoir Terra Simulator
[2] Petrel, version 2017

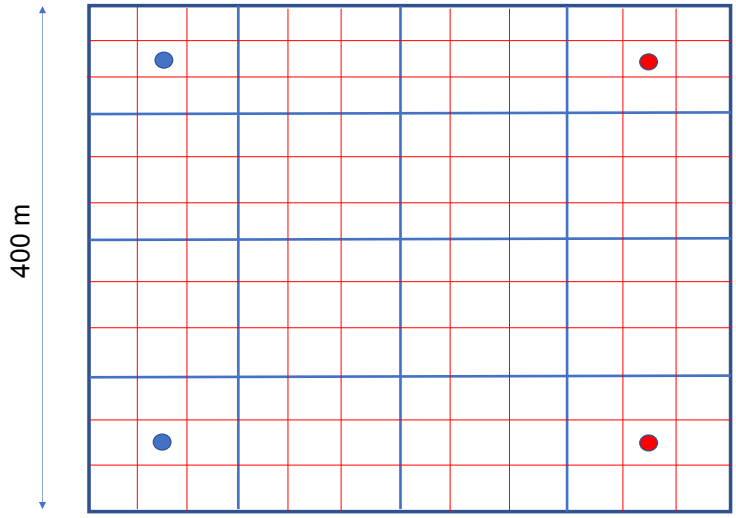

Figure 3.1: well location consistency in model discretization. The blue and the red circles represent the producers and the injectors respectively. The initial model is a 4 by 4 by 1 square which each cell is divided into 3 by 3 cells to increase model resolution.The discritization process continues until reaching adequate resolution for the reference model which is 108 by 108 in this case. Wells are located at the center of each grid cell and the spacial distance between wells is kept consistent.

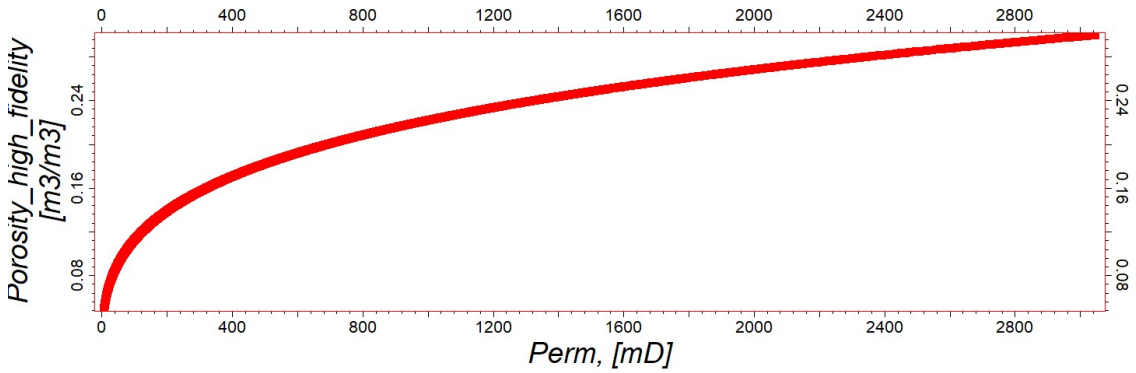

Figure 3.2: The porosity-permeability relationship for one the realizations for the reference model. The Karman-Cozeiny correlation with average grid size of $1E^{-8}$ meter and tortuosity of 180 are used to develop porosity-permeability relationship.

and graphical illustration of the porosity-permeability relationships respectively

$$K_{absolute}(mD) = 55555.5\frac{\phi^3}{(1-\phi)^2}. \tag{3.1}$$

The fluid PVT model is kept as simple as possible which is shown in table 3.1 for the pressure of 1 bar and the rock/fluid properties such as relative permeability is considered to be non-linear as follow:

$$n_w = 2, n_o = 2, K^e_{rw} = 1, K^e_{ro} = 1, S_{wc} = 0.15, S_{or} = 0.2. \tag{3.2}$$

	oil	water	rock
viscosity (cp)	1.29	1	-
compressibility (1/bar)	4.5E-7	4.5E-7	1e-5
Formation volume factor (m3/m3)	1.02	1	-
Solution gas oil ratio	0	0	-
Density (kg/m3)	800	1000	-

Table 3.1: PVT and rock properties of the reference model

3.2. Structured Proxy Model

For the synthetic reference model, the proxy model is created using the same scheme used for the reference model. The model is discretized with DARTS and the coarsening procedure for increasing the resolution of the proxy model is quite equivalent to the discretization of the reference model, however, the proxy resolution is 9 times smaller (12 by 12 by 1). As explained in section 3.1, the well's locations are consistent in the coarsening process to keep the spatial distance constant between wells. As for the petrophysical properties, the *Geometric Upscaling* method is used to upscale the properties (porosity in this case) in the fine model grid cells to their corresponding course grid cell. The *Property Upscaling* feature in Petrel is used to conduct geometric upscaling. Figure 3.3 illustrates the fine and the course model porosity distributions after the upscaling procedure. During the upscaling process, some of the porosity values for some of the grid cells might be effected by the averaging operation, thus the porosity distribution for the reference model would be different comparing to that of proxy. Figure 3.4 depicts the porosity distribution histogram for the reference and the proxy model for one of the realizations.

The permeability of the upscaled model could be generated in various forms. Geometric averaging for the flow properties is not accurate enough to represent the property distribution in the reference model, therefore, flow-based upscaling methods can be utilized to approximate the values of permeability in the courser model. In this approach, since the flow-based upscaling might need an extensive pre-knowledge of the reservoir fluid flow, the same Karman-Cozeiny correlation is used to evaluate initial permeability distribution for the proxy model.

3.3. Data-driven Model for Synthetic Reservoir

In this section, the outcomes of the various experiments on the performance of the optimizer will be demonstrated and discussed for the synthetic 2-dimensional model. Different reservoir heterogeneity is tested and the reconstruction ability of the optimizer will be examined with various initial guesses and production strategies. As discussed in section 1, the purpose of building a synthetic model is to generate the true response of a reference model and investigate the effect of various initial guesses on optimization performance. The approaches and methods used in creating 2-dimensional reference model are explained in detail in section 3.1.

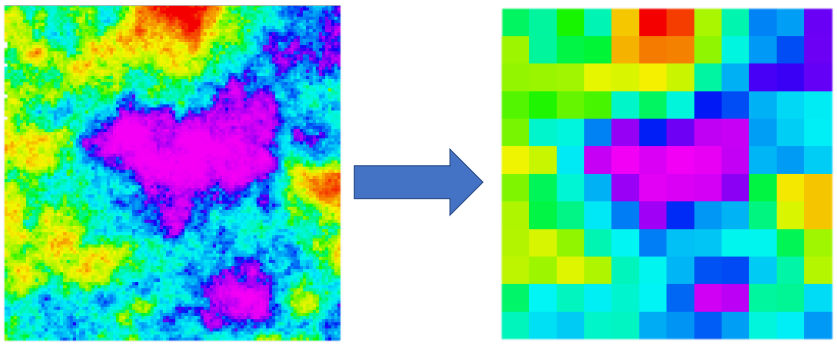

Figure 3.3: The left picture represents the reference model (i.e. the high-fidelity model) porosity distribution modelled by *Gaussian Random Simulation Function* which is constrained to the synthetic well logs. The right picture is the upscaled porosity of the proxy model which is the volumetric (Geometric) average of the corresponding fine cells in the reference model.

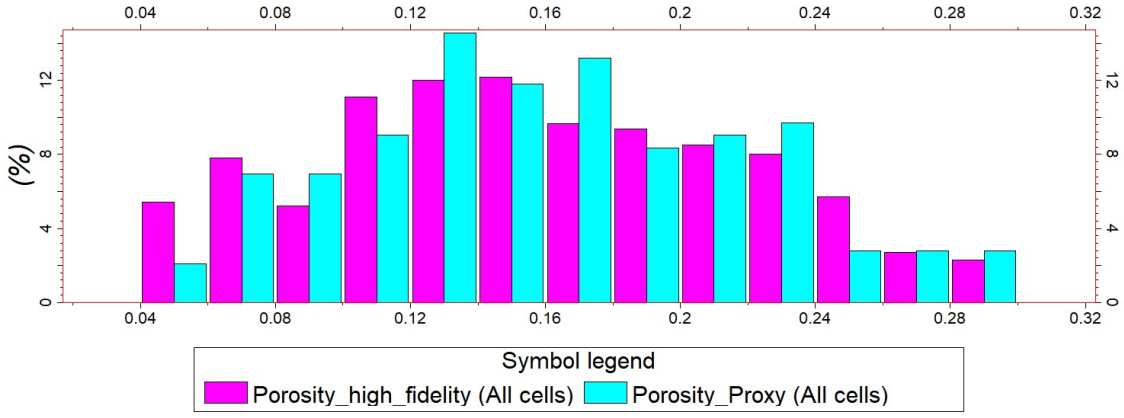

Figure 3.4: The porosity distribution histogram for the reference model(i.e. the high-fidelity model and the proxy model. The high-fidelity model is 108 by 108 and the proxy is 12 by 12 grid cells.

3.3.1. Single Region Heterogeneity with Perturbed Initial Guess

The term *Single Region* indicates that the entire reservoir has single permeability average which is distributed over the grid cells with normal perturbations. For instance, 0% perturbation reveals homogeneous permeability distribution in all cells while 10% perturbation means the permeability is distributed with the similar average permeability and normal perturbation of 10 percent. It is worth to mention that in the all cases, the locations of the producers are set in the high-permeable zone and the injectors in the low-permeable zone in which all of them are controlled by random perturbed BHP. The performance of the optimizer is examined with the **fluid rate mismatch** (i.e. the misfit between initial guess and the true response compared to misfit between the optimized model and the true response) and the number of **iterations** optimizer takes to converge.

The primary rate misfit results of the single region heterogeneity with various initial guess perturbation are illustrate on figure 3.5. The effect of the perturbation of the permeability in the initial prior model can be observed by following the gray lines in the figure 3.5. The misfit performance of each perturbation seems to be the same as one another, however, the computational time (i.e. the optimization iteration) that each example took to converge is different. According to figure 3.6a, the number of iterations tends to increase as the perturbation of the initial guess raises. The perturbation of 0 and 2 percents are exception from the general trend and this is because of the limitation of the optimizer to deal with very close initial guesses. The overall error is shown on figure 3.6b which does not follow a specific trend. Since the overall error is below 0.1 percent, the comparison of the overall errors are not reasonable with only a small perturbation in the initial permeability. Therefore the only parameter to compare cases is the computational cost or the number of optimization iterations.

To conclude, in a single region permeability model, the more perturbed initial guess is used, the more iteration the optimizer takes to converge. While the overall error is below the threshold point of 0.1 percent, all the proxy models are in acceptable convergence range. This conclusion might be different with more heterogeneous and more complicated reservoir models.

3.3.2. Heterogeneous Model with Perturbed Initial Guess

In this part, a 4-region permeability reference model is used to analyse the optimizer's performance with various perturbed initial guesses. The perturbed permeability values are scattered with normal distribution methods in each region individually, and wells are located at the consistent location in the middle of each region. The values of the average mean permeability used in each region are 100, 200, 500, and 50 mD. In all the cases, the producers are at the high permeable zones and are control by random perturbed BHP.

Figure 3.8 depicts the oil rate versus time for the true response (red dots), trained model (blue line), and the prior guess (gray line) for prior perturbations of 0, 2, 20, 30, 50, and 100 percent. In the 4-region heterogeneity model, the permeabilities' perturbation is more visible than the single region model. In all the cases, the optimization procedure successfully trained the prior guess; however, the computational effort for each guess is different. Figure 3.7a represents the number of iterations that the optimizer took to converge in each prior. Obviously, by increasing the perturbation of the prior guess, the number of iterations increases. As mentioned previously in section 3.3.1, the reason behind discontinuity in the number of iterations in perturbation 0 and 2 per cent is the limitation of the optimizer to converge a very close initial guess to the true response. Since the history matching process is an ill-posed problem, it took an additional effort for the optimizer to find the solution for a very similar guess to the true values. Comparable to the previous single region experiment, the overall misfit error is below the threshold value of 0.1 per cent for the simple models; thus, comparing the misfit errors are not reasonable.

By investigating the optimization performance in a 4-region permeability model, which can be considered as a reasonably heterogeneous reservoir, it is proved that the effect of the initial prior geological knowledge is significant in terms of computational cost. Therefore, an adequate initial guess for the optimizer in constructing the data-driven model is crucial and can reduce the computational time to a large extend. The 4-region permeability experiment was quite a small test for the DiWA model, and

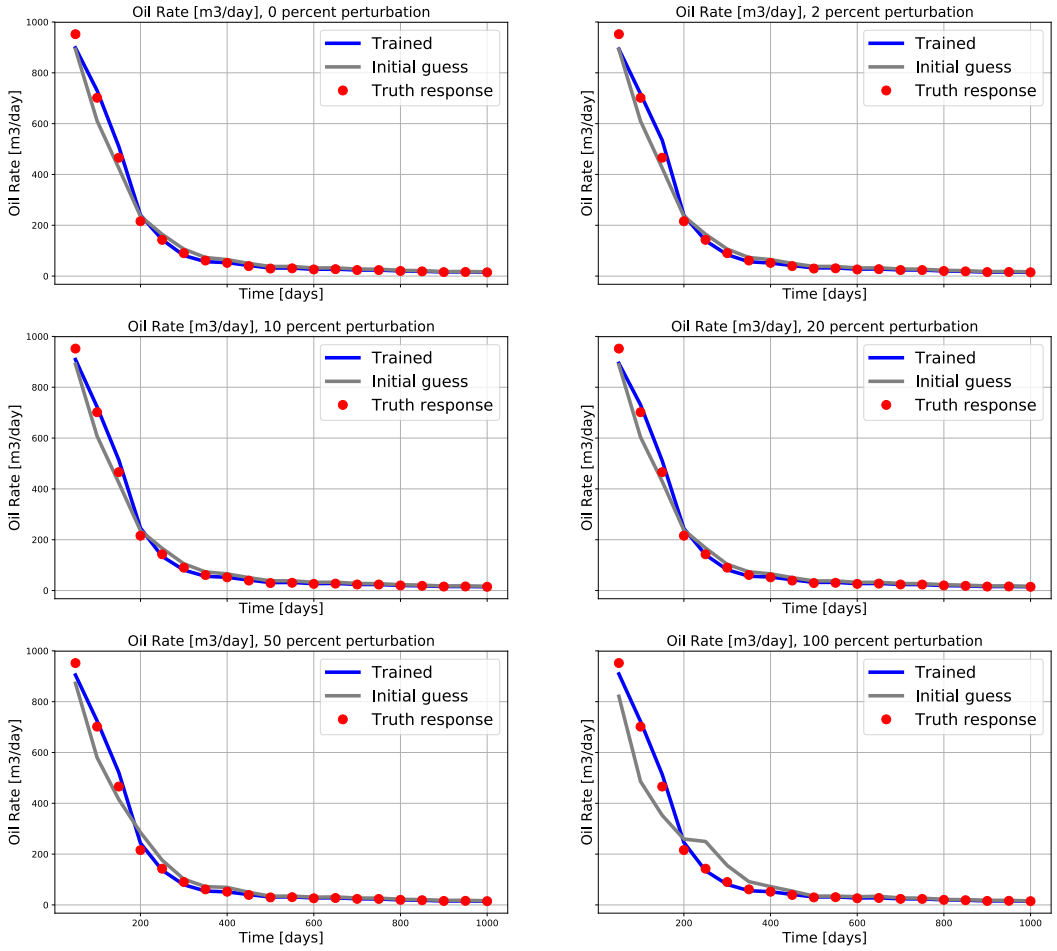

Figure 3.5: Single Region Heterogeneity training results for the simple 2-dimensional 108 by 108 reference model and 12 by 12 structured proxy model. The red dots are the reference model response (true oil rate), the blue line the trained oil rate and the gray line is the initial guess with perturbation of 0, 2, 10, 20, 50, 100 percent.

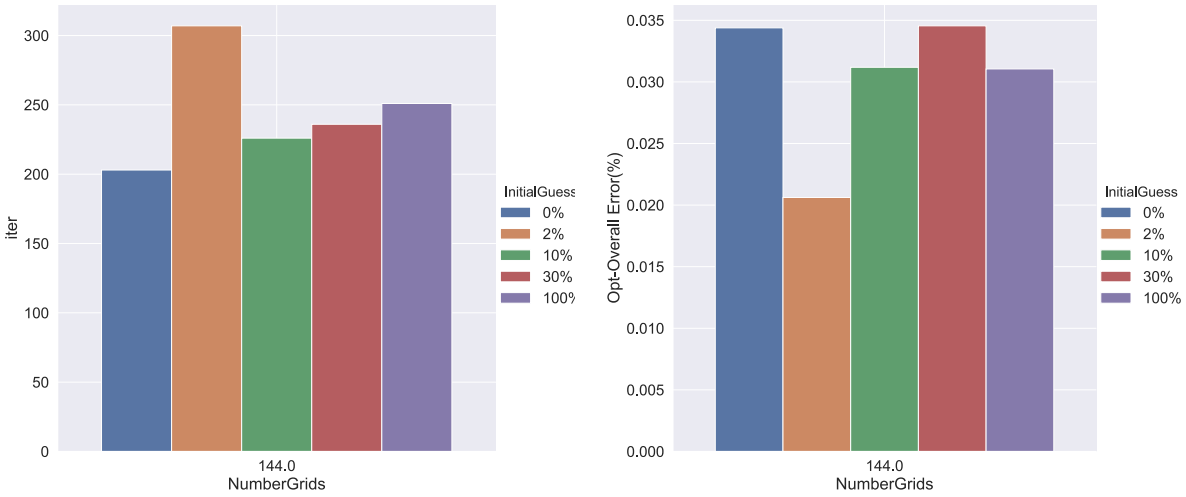

(a) Optimization Iteration

(b) Optimization Overall Rate Misfit

Figure 3.6: Single Region Heterogeneity optimization performance for the synthetic 2-dimensional 108 by 108 reference model and 12 by 12 structured proxy model. Bar chart (a) represents the number of iterations that the optimizer took to converge for various perturbed initial guesses. The bar chart (b) illustrates the overall L-2 norm misfit error of the true response and the proxy response.

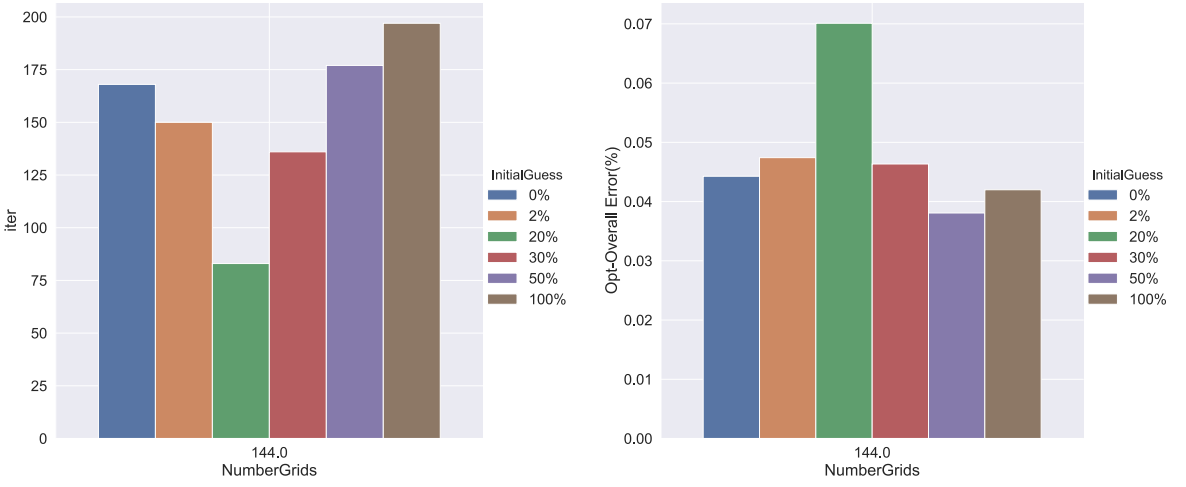

(a) Optimization Iteration

(b) Optimization Overall Rate Misfit

Figure 3.7: This graph represents the results for the 4-region heterogeneity training performance. The synthetic 2-dimensional 108 by 108 reference model and 12 by 12 structured proxy model is used for this simulation results. Bar chart (a) represents the number of iterations that the optimizer took to converge for various perturbed initial guesses. The bar chart (b) illustrates the overall L-2 norm misfit error of the true response and the proxy response.

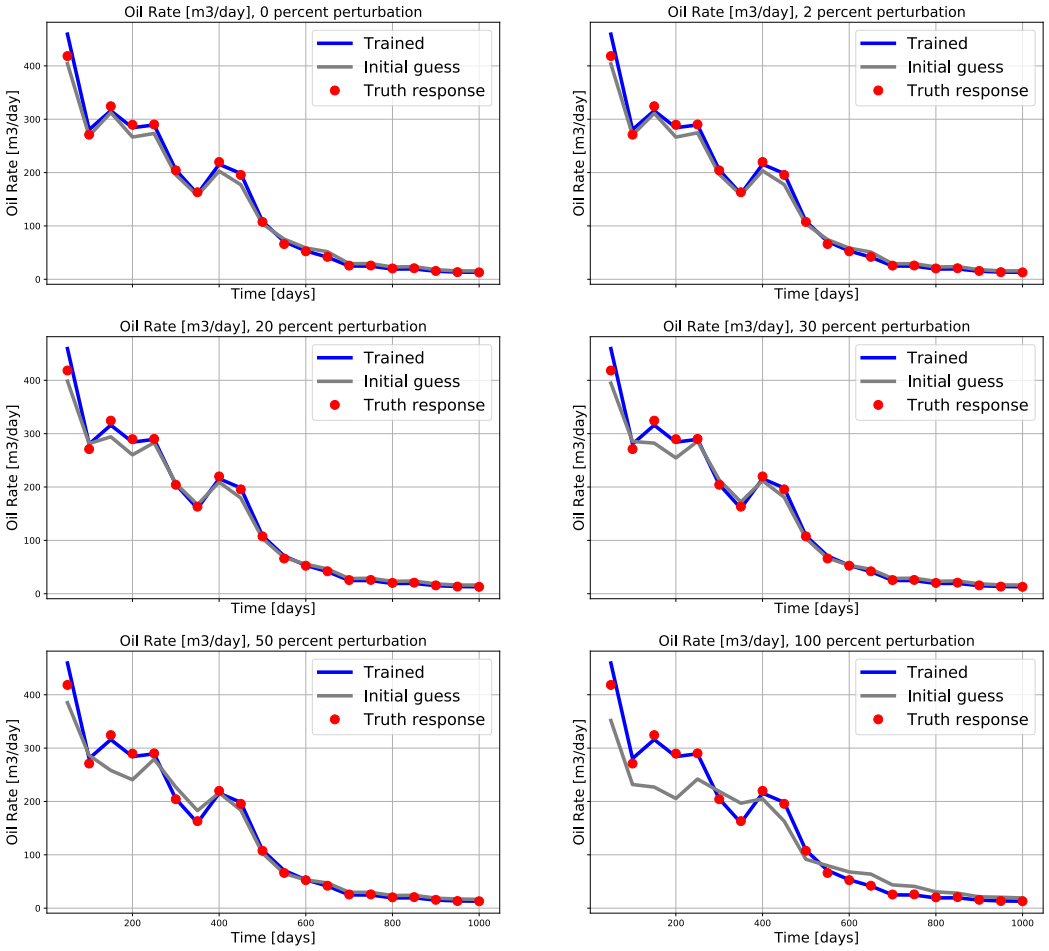

Figure 3.8: 4-Region Heterogeneity training results for the simple 2-dimensional 108 by 108 reference model and 12 by 12 structured proxy model. The red dots are the reference model response (true oil rate), the blue line the trained oil rate and the gray line is the initial guess with perturbation of 0, 2, 20, 30, 50, 100 percent.

optimizer performance should be analyzed with larger models and realistic data.

In this part of the study, the petrophysical properties (e.g. permeability) are assigned in each region individually with normal distribution; however, in reality, the geological properties are modelled with stochastic modelling methods, which are constrained to the well information (i.e. extrapolated by well log data). In the next part, the optimization performance and the ability of the framework to reconstruct the geological reference model with several stochastic prior realizations are investigated and compared to the deterministic approach of perturbed priors.

3.3.3. Reconstruction of the Reference Model with Deterministic Approach

The ability of the optimizer to reconstruct the reference reservoir parameters (i.e. model parameters to be trained, such as transmissibility, well indexes and Corey parameters) is crucial to find out the presence of the unique solution. This experiment uses the 4-region permeability reservoir as the reference model to train the structured proxy with various perturbed prior guesses. After the optimization procedure, the trained parameters of the proxy model is converted to permeabilities at the interfaces of each two grid block and compared to the prior guess. It is worth mentioning that the permeability values at the boundary of each region are removed from the outcomes because a significant jump of the permeability from one region to another may give unreasonable solutions by the optimizer. Final results are illustrated as error bars of permeabilities for both prior knowledge and the trained model. All the well controls and production strategies are similar to section 3.3.2.

Since a single prior model with only some perturbations around the true value is used, the approach taken in this section is called the *deterministic* approach. The expectation from the deterministic approach is a significant improvement in the deviation of the permeability in the trained model comparing to the prior knowledge. If the optimizer can reconstruct the reference model with a small perturbation of the prior guess, we can claim that the solution of the training process is unique, and the optimizer can find the optimum global solution. Figure 3.9 illustrates the permeability's **standard deviation** in each region for the prior and the trained models. As it is clear, the optimizer has converged with permeability values far from the original reference permeability. For instance, in the outcomes for the 30-per-cent perturbed prior model in region 1, the standard deviation of the trained model (green line) is larger than the 30-per cent perturbed prior model (red line). On the other side, according to figure 3.7b, the overall error of the 30-per-cent perturbed model is tiny, which means the optimizer successfully matched the prior model to the true response. Consequently, this experiment proved that the DiWA framework could not reconstruct the reference model with a direct initial guess.

Considering the outcomes of this experiment, perhaps the contributing reason justifying the disability of the DiWA to reconstruct the reference model is the ill-posedness of the inverse problem. The *ill-posedness* or the *non-uniqueness* means that there are several possible solutions (i.e. several completion of the modifiers can converge to optimum solution) for a single problem to match the observed data. These results indicate that the inverse problem is significantly dependent on the prior information fed to the optimizer; thus, further considerations are required to guide the optimizer to the target optimum [3] solution. One possible method to resolve this issue would be the *Model Reparametrization* or *Model Regularization*, which limits the objective function to the target optimum solution by using several realizations as prior knowledge. Before approaching the parametrization methods, the DiWA model is tested with the more realistic prior realization, which is discussed in section 3.3.4.

3.3.4. Reconstruction of the Reference Model with Stochastic Approach

It is shown in section 3.3.3 that the *Deterministic* approach is not effectively reflecting the optimization performance since the basis of a history matching problem is ill-posed; therefore, the solution is not unique. Limiting the problem to the reference solution by adding the regularization term to the objective function (described in section 2.2) might be applicable in such cases; however, applying several prior

[3] Target optimum means the solution in which the trained reservoir parameters are close to the reference reservoir model

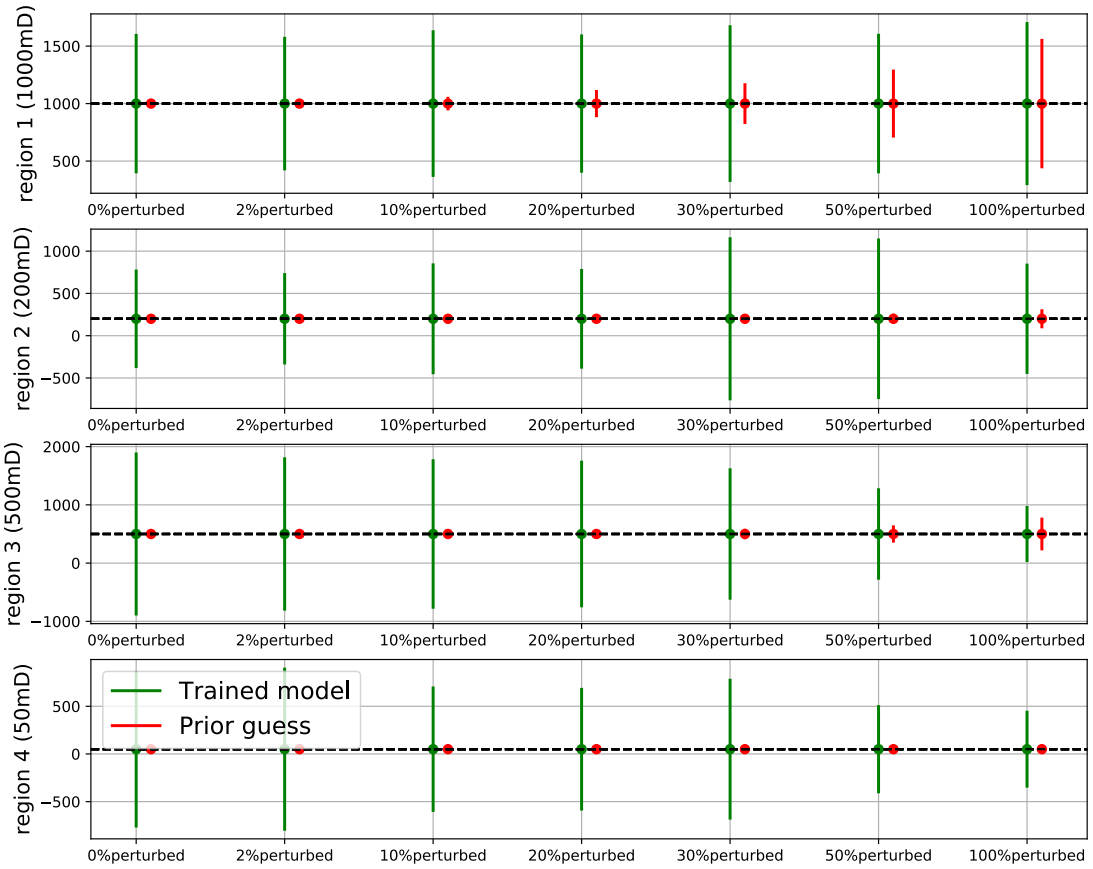

Figure 3.9: This graph analyzes the ability of the DiWA model to reconstruct the reference model. The 108 by 108 reference model and 12 by 12 proxy model are used for the 4-region permeability distribution. The green and the red lines represent the standard deviation in a single region after and before the training, respectively. These results came with an overall rate misfit error of 0.06 per cent, which indicates a reasonable match of the production rates. The graph also explains the disability of the optimizer to reconstruct the reference model properties with a single prior guess. Note that the values of the error lines are the standard deviation, so negative values of the permeabilities do not indicate the permeability itself but the deviation.

guesses (here are permeability realizations) can result in acceptable reconstruction performance of the DiWA model.

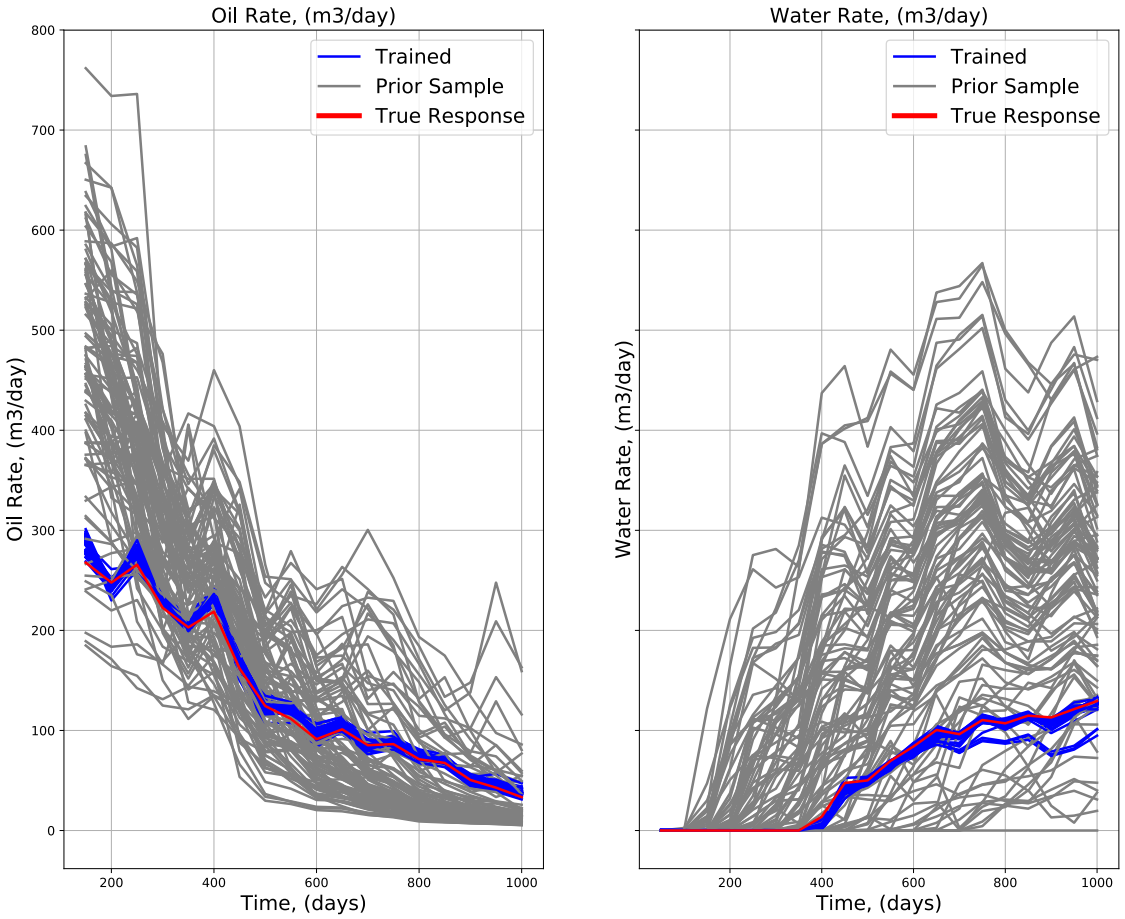

Figure 3.10: The oil and water rates simulation results for the reference (the true response), the prior (100 realizations) and the trained models. Simple 2-dimensional 108 by 108 reference model with 12 by 12 structured proxy model is used in this experiment. Priors are created by stochastic property modeling methods, which are constrained to the synthetic well log information. The objective function is constructed with both oil and water rates and wells are controlled by random BHP.

To investigate the proposed *Stochastic* approach, 100 permeability realizations are created using synthetic well log information in the so-called simplistic 2-dimensional reference model. The priors are created using the stochastic property modelling method of *Sequential Random Gaussian Simulation*. After training the proxy with 100 realizations as prior knowledge, the optimizer's performance is checked with overall misfit rate error and all of them are confirmed to match the oil and water rates. The reconstruction ability of the model is then assessed by examining the histogram of the permeability at the specific two grid cells interface in the 100 priors and corresponding trained models. The initial expectation from this experiment is that the permeability distribution (i.e., permeability histogram) of an individual interface of the trained models becomes closer to the reference model permeability.

Figure 3.10 illustrates the oil and the water rate simulation results for the true response, the initial guesses and the trained models for 100 distinct permeability realizations. As it is clear from the figure 3.10, the optimizer performed accurately in training the proxy models for the production time of 1000 days. The overall rate of misfit error for all 100 test cases are below 0.2 per cent; therefore, the

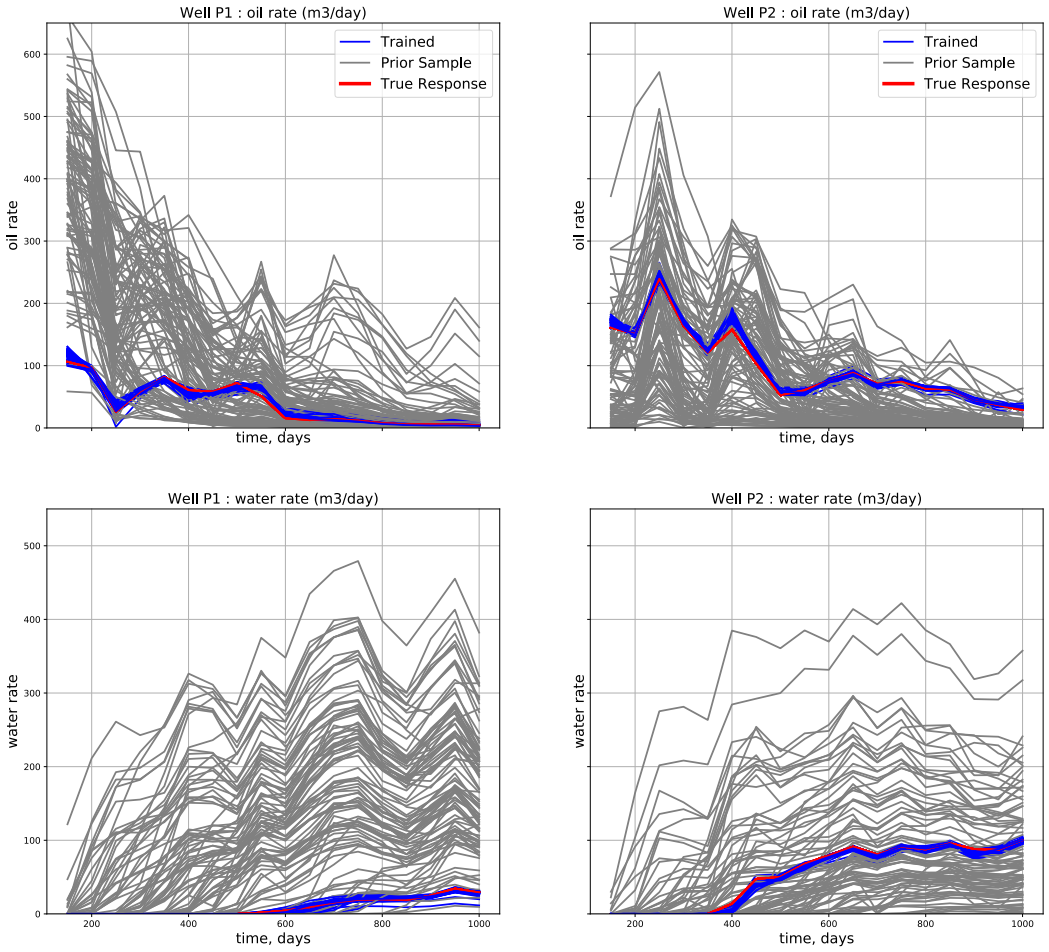

Figure 3.11: The oil and water rates simulation results for the reference (the true response), the prior (100 realizations) and the trained models for each production well. Simple 2-dimensional 108 by 108 reference model with 12 by 12 structured proxy model is used in this experiment. Priors are created by stochastic property modeling methods, which are constrained to the synthetic well log information. The objective function is constructed with both oil and water rates and wells are controlled by random BHP.

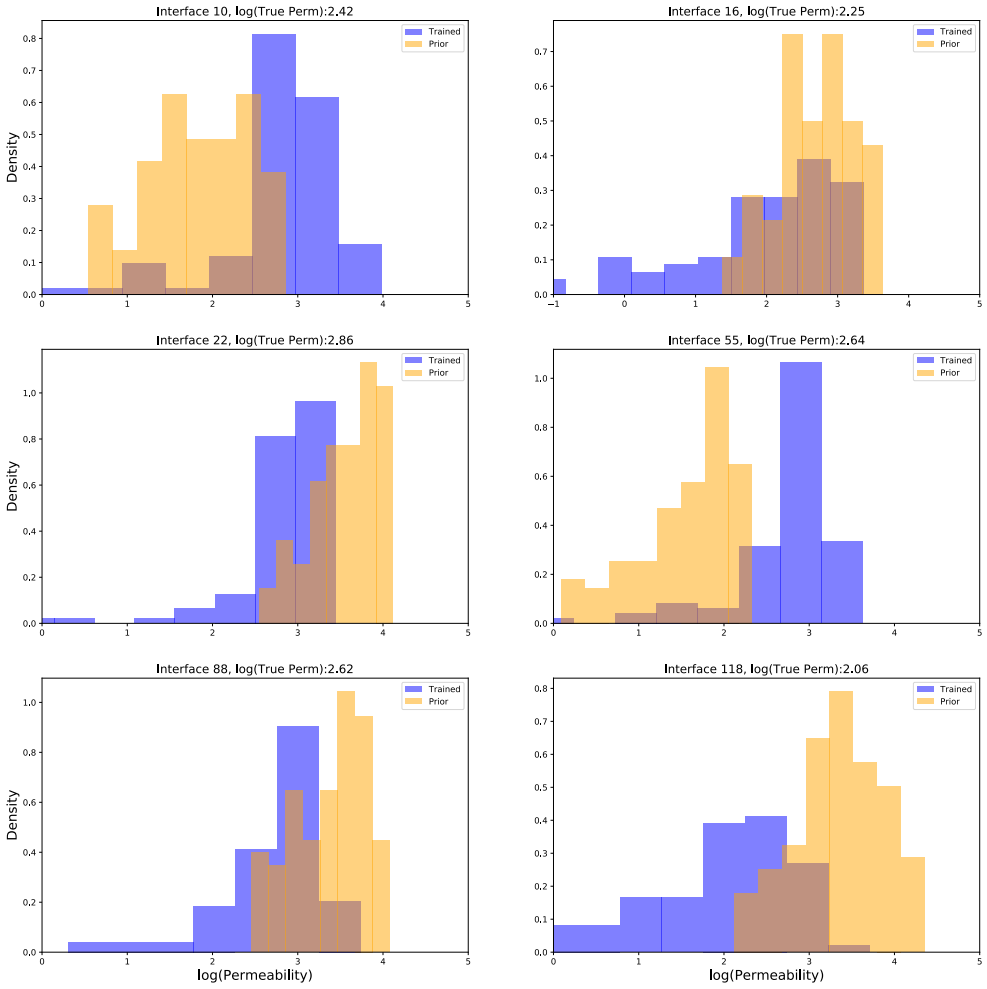

Figure 3.12: This graph illustrates the logarithmic histogram of the distribution of permeability at the six random interfaces for 100 realizations. It also shows the ability of the DiWA model to reconstruct the permeability of the reference model despite the ill-posedness origin of the framework. The logarithmic value of the true permeabilities correspond to the reference high-fidelity model are demonstrated at the top of each sub-graph.

performance of the training procedure is acceptable. Representing the optimization performance with only field total fluid rate might eliminate some of the trained outcomes; thus, for adequate investigation, the separated oil and water rates simulation results for the true, prior and trained models for each production well are demonstrated in figure 3.11. The optimizer could train the proxy model accurately in almost all the prior guesses in each well.

The ability of the DiWA model to reconstruct the reference model permeability map is depicted in figure 3.12. In this logarithmic histogram, the number of six proxy model interfaces are randomly selected, and the distribution of the permeability at the interfaces for 100 realizations of the prior and the trained model is shown. The first point that can be interpreted from the figure 3.12 is that the histogram of the trained models is more broadly distributed than that of the prior models. This observation indicates that a broader range of permeability values can be considered the optimum parameter for the optimizer when converging to true reference response. This wider shape of the trained histogram is a clear indication of the ill-posedness of the problem.

By comparing the histogram of the trained model to the prior guess, it can be understood that the distribution of the trained model is shifted to the true reference value of the permeability (the logarithmic value of the reference permeability is demonstrated at the top of each graph). The picks (i.e., higher density) of the histogram of the trained model are mostly assigned to the true permeability value meaning that most of the trained priors are converged to the vicinity of the true permeability values. It is worthy to mention that the quality of priors selected are crucially importance in this experiment; if the priors are not close to the true permeability, the optimizer will converge to another optimum.

Overall, these results indicate that the DiWA model can perform effectively with given close priors to the true permeability (figures 3.11 and 3.10); however, the optimum solution corresponding to the reference model is not always achieved. According to the outcomes delivered by figure 3.12, through using various realizations constrained to the well information, the DiWA model is capable of developing the reference model permeability even without conducting regularization. On the other hand, the effect of prior knowledge on the optimization performance becomes more significant when aiming to reconstruct the reservoir parameters. In this research, the prior guess is picked from various realizations from the exact statistics of the reference model; thus, the optimizer could statistically converge to the reference model. In conclusion, the prior knowledge in the training performance is crucially important since the behaviour of the optimizer in selecting local optimums depends on initial parameters fed to the DiWA model. It can not surly proven that in all the cases the framework can converge to the reference model since there are several other factors contributing in a history matching problem.

4

Realistic Oil Field

In this chapter, first, the method and the theory used to create the field proxy model is discussed in details. Afterwards, to evaluating a realistic data-driven model for a reservoir, the oil field [1] production history and geomodel model is described in brief and the procedure building of unstructured proxy model is explained as well. Finally, the results and the analysis of the outcomes are demonstrated and discussed from various perspectives.

4.1. Oil Field Model

In this study, a real oil field is used as a realistic case to investigate the performance of the data-driven approach on real-life field data. For the mentioned purpose, in addition to the geological static model, rock/fluid properties, and the production history of the target reservoir, the well path and completions are also required to build the proxy model.

4.1.1. Structural Properties

As a general information about the oil field, the size of the entire rectangular model is in the range of 1500 by 500 meters. The reservoir consists of nine layers with two pay zones which are relatively disconnected to each other by an impermeable zone in between. Furthermore, there is an active water aquifer below the lower zone which provide relatively effective water drive mechanism for oil production. The reservoir encompasses a major normal fault (called *Central-HC* fault) along the North-East to South-West direction which is assumed to be a sealing fault against the fluid flow. In addition to the Central-HC, there are some smaller crossing faults in various directions which are not considered as impermeable as the Central-HC fault. The reservoir is located at the datum depth of 640 meters with the net thickness of 103 meters. The top of the reservoir is 550m deep and the Water-Oil Contact is located at the depth of 653m. The entire high-fidelity model is discretized with 1,891,351 uniform structured grid cells in which some of the cells are set to be non-active cells in the simulation.

4.1.2. Wells

Overall, the field contains 61 wells in which 43 of the them are producers and 18 wells are injectors. It is worthy to mention that there are 13 horizontal wells out of 43 producers and 3 horizontal wells out of 18 injectors. As for the completion design for the wells, all the vertical wells are cased-hole with perforations in the upper, lower or both pay zones. The horizontal wells are completed as open-hole

[1] The term the *Oil Field* refers to a realistic oil field data and model.

well and in some cases, the well is squeezed to maximize the production and strengthen the well. There is no additional data on well stimulation or damages, thus zero skin factor is assumed for all the wells. There is no downhole gauge to measure fluid rate or track the Bottom Hole Pressure (BHP) along the field history, therefore, production data might be significantly affected as the are collected from the separator at the surface.

4.1.3. Petrophysical Properties

The geological model was build with seismic interpretations and well log analysis. Properties such as Net to Gross (NTG), porosity, and water saturation are modeled with geo-stochastic simulator which are constrained to the well and the seismic data. The well logs are not available, thus a new geological interpretation for reservoir properties couldn't be conducted in case of creating several realization. In total, there are three porosity-permeability correlation for the two pay zones and the water aquifer. The aquifer is more permeable even in lower porosity values, however, the lower pay zone shows wider variability of permeability versus porosity with smaller values comparing to the aquifer. The upper pay zone is something between the aquifer and the lower zone in a way that the permeability values are more moderate and alter more uniformly with porosity.

As for the NTG and water saturation, the aquifer (because the water saturation is higher) and a thin layer between two pay zones (i.e. an impermeable shale layer) are excluded from the volumetric calculations of initial fluid in place and the fluid flow in the simulator since they are not considered as reservoir rock (i.e. NTG = 0). The saturation distribution in two pay zones are different from one another. The upper zone consists less initial water saturation comparing to the lower zone and this fact is due to the connectivity of the lower zone to the active aquifer. The capillary pressure and the wettability property of the rock might affect the water saturation, however, the magnitude of the capillary transition zone is negligible due to its small magnitude.

The relative permeability of the oil reservoir is determined with core analysis and it is represented by Brooks-Corey model. Overall, the reservoir is water-wet with connate immobile saturation of 0.16 and the end-point water relative permeability of 0.15 at $S_w = 0.8$ which means that the mobility of water is very low. The end-point relative permeability of oil is 1 at $S_w = 0.16$ which indicates the higher mobility of oil just in terms of relative permeability as it is illustrated by figure 4.1. The total mobility of the fluid depends on the effective permeability and the viscosity of the fluid. The oil of the target reservoir is quiet heavy with dynamic viscosity of $93centi - poise$ at the reservoir condition of $94bar$ and $45C$. According to the figure 4.2, the mobility (i.e. the ratio of effective permeability to fluid viscosity) of oil is higher than water at water saturation below 0.4 and then the mobility of water increases rapidly as the water saturation raises. Consequently, despite the low relative permeability of water, the mobility of oil tends to decrease to values far more smaller than the mobility of water. It is worthy to mention that, all the previous interpretations of the mobility are at the reservoir initial condition and as the production continues, the behaviour of the fluid properties will change as the pressure in the reservoir changes.

4.1.4. Volumetric Properties

In order to evaluate the *Standard Total Oil Initially In Place (STOIIP)* calculations, some reservoir parameters are required. Utilizing the NTG, irreducible water saturation (S_i), the total porosity and the Recovery Factor (RF) the STOIIP calculations can be perform on every grid cell. It is tried to make the proxy STOIIP and the original segmnet equivalent to each other by adjusting parameters such as porosity, net-to-gross or initial saturation. The detail information of volumetric properties of the target reservoir is explained on table 4.1 .

4.1.5. Developing Strategies and Well Controls

The production strategy used in this reservoir encompasses only water flooding with the starting point at the time of primary depletion (at approximately 7000 days/20 years after the first production well)

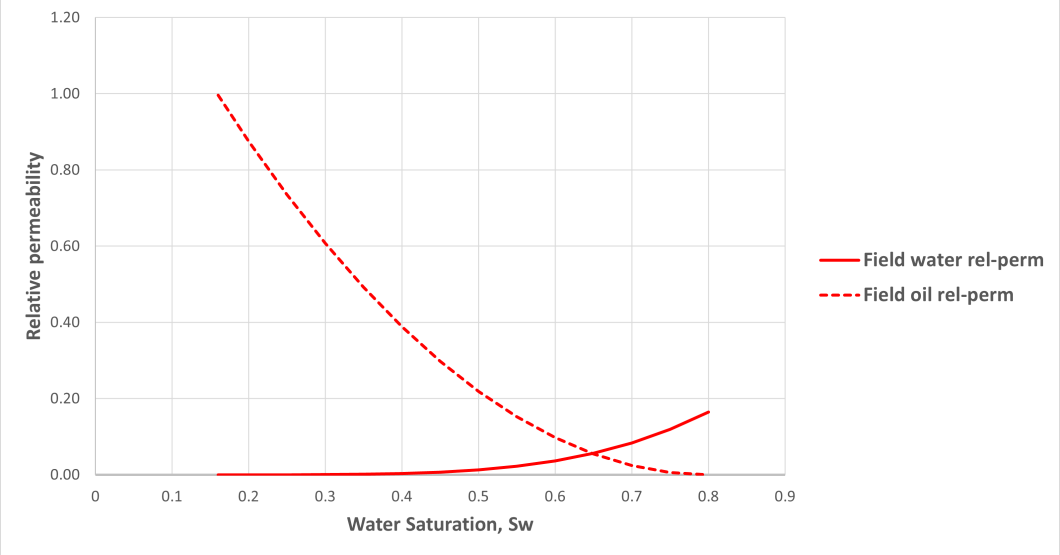

Figure 4.1: Field relative permeability curves.

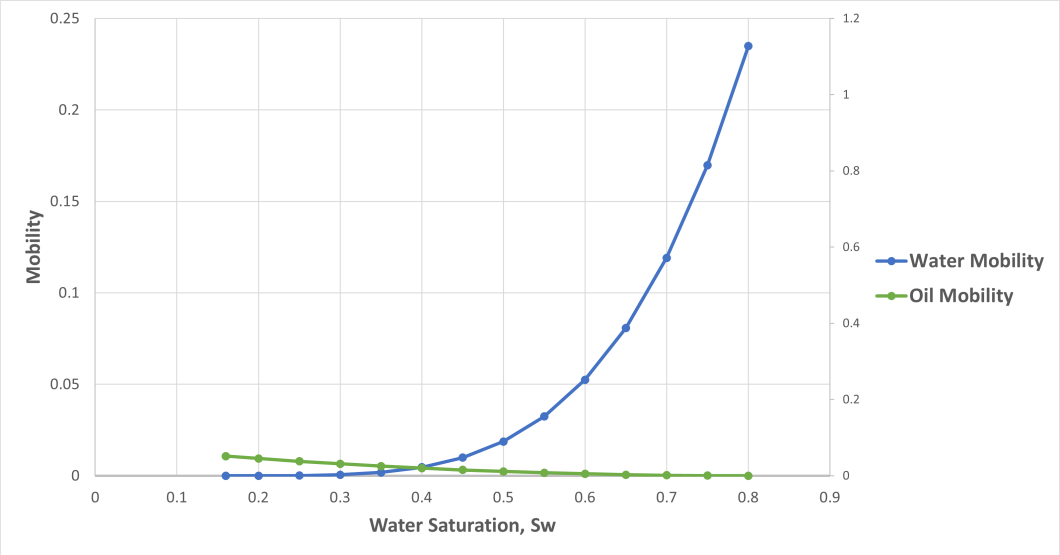

Figure 4.2: Field mobility curves for oil and water.

	Bulk Volume (m3)	STOIIP (m3)
Segment 1	120204670	6737327
Segment 2	86706346	5840227
Segment 3	31646430	1895080
Segment 4	14365769	739310
Segment 5	11919590	678630
Segment 6	7913517	398199
Segment 7	1045976	404459
Segment 8	3065365	8929
Segment 9	998419	28452

Table 4.1: The bulk volume and the STOIIP of the oil reservoir categorized for each reservoir segment.

of the reservoir. Both vertical and horizontal wells are used for the flooding operation and they are completed mostly close to the aquifer-reservoir boundary at the lower payzone and at the bottom of the upper payzone. Existence of various faults in the reservoir has made the flooding pattern slightly different as some of the faults are sealing and impermeable to fluid flow. The water breakthrough time is very close to the injection starting point which reveals that the mobility of water increased significantly as the water saturation raises with the flooding process. Figure 4.3 represents the field oil and water production recorded with the reporting time step of 30 days. As it is clear from the figure 4.3, the primary depletion of the reservoir starts at about 2500 days and the injection operation begins at 7000 days to compensate the depleted pressure.

Figure 4.3: The upper graph represents the raw Field Total Oil Production with primary depletion at 2500 days and production enhancement at 7000 days with water injection. The lower graph illustrates the raw Field Total Water Production with breakthrough at approximate time of 7200 days. The reporting time step is 30 days for both graphs

4.2. Unstructured Proxy Model

In order to build a proxy model for the oil field, an unstructured discretization system is selected to perform as the structure of the reservoir. The unstructured grid system is suitable for heterogeneous reservoirs with complicated geometries and connections, therefore, for future advance application of the proxy model, the unstructured discretization is used for creating cells transmissibility and the connection list. In this section, a detailed description of the proxy model for the oil field is explained and all the strategies for resolving oil field data outliers and simulator convergence issues are pointed as well.

4.2.1. Unstructured Grid Mesh

As explained earlier, the unstructured grid system has a main advantage of covering complex geology and heterogeneity such as highly fractured reservoirs and able to evaluate fractures transmissibilities as well. For the oil field proxy model, the Gmsh tool [10] is used to create unstructured grid cells with the volumetric shape of prisms. For instance, the unstructured grid system for the segment 2 of the oil field is depicted on figure 4.4 which has 2 layers and each contains 189 prisms (i.e. 378 prisms in total). From the unstructured mesh created by Gmsh, the bulk volume, reservoir boundaries, vertical and horizontal resolutions and the approximate equivalent well grid cells can be interpreted.

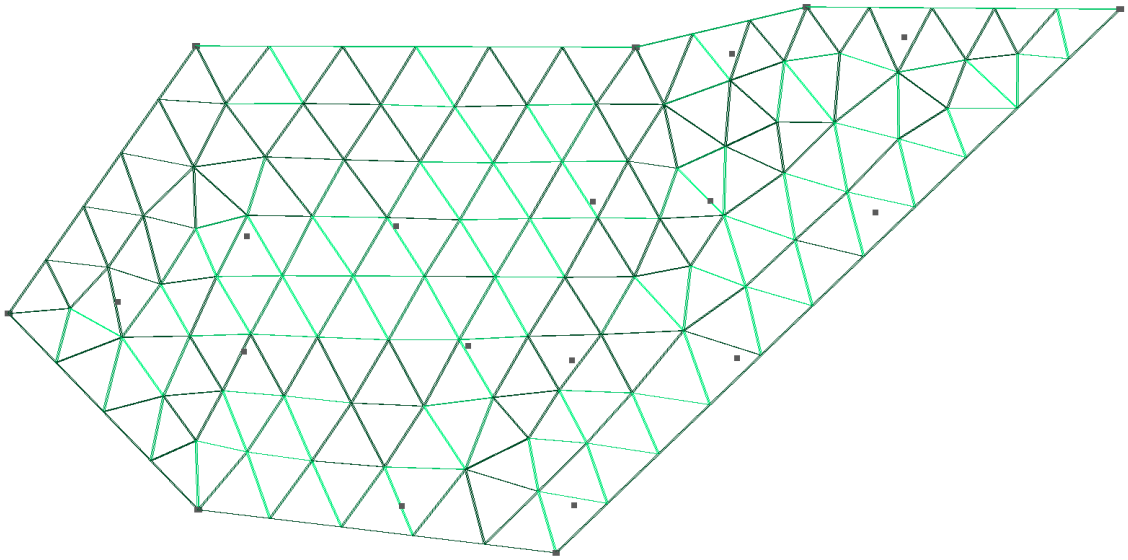

Figure 4.4: The Segment 2 Unstructured grid system of the proxy model for the oil field generated by Gmsh tool. It include 2 vertical layers with 189 prisms in each layer. The size of each prism is not equivalent to one another. The black dots represent the location of the wells in the segment of interest.

4.2.2. Petrophysical Properties

Since the porosity and the permeability of the reference oi field is already modeled and validated with well logs, the petrophysical properties of the proxy model can be evaluated from the reference model. In this framework, there are two methods projecting the porosity and the permeability from the reference model to the proxy model:

- **Random Statistical Upscaling**: The reference model contains the statistical properties of the porosity and permeability model, therefore, by using the property's mean and the standard deviation, a random sampling from the property distribution can be a reasonable prior knowledge for the petrophysical properties of the proxy model. The main advantage of this approach is the simplicity and the availability of the mean and standard deviation in most of the geological models, however the downside is that this method is not upscaling the property based on the location and cell volume. In the stochastic data-driven approach, various realizations can be easily generated with this approach.

- **Volume-weighted Geometrical Upscaling**: As it is explained in section 2.5.2, the geometric upscaling method requires cell volume and the cell corresponding property. In order to get reference model cells inside each prism, a Python code is developed to find the reference model

cell indexes inside the volumetric space of each prism in the proxy model. Afterwards, by having the reference model cell index and the corresponding property, the upscaled value of the property for the unstructured system can be calculated. Perhaps the major upside of this method is that it will produce an effective initial guess with a close estimation of geological properties to the reference model. Besides, this approach will constraint the petrophysical properties to the well information and reduce the property modeling uncertainty to a large extend. For instance, figure 4.5 compares the porosity map of the unstructured grid proxy calculated using volume-weighted upscaling method and the field geomodel porosity map.

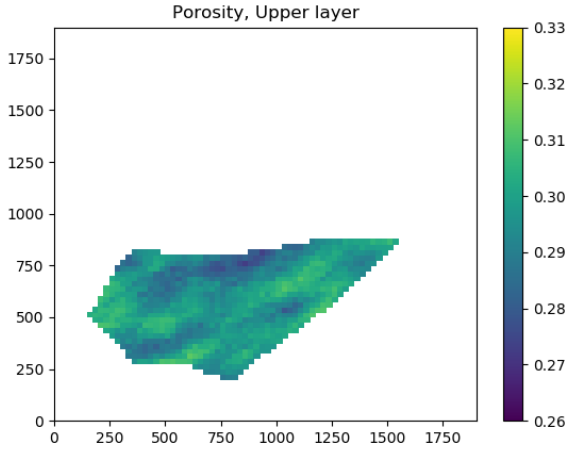

(a) Original field porosity map of the upper layer

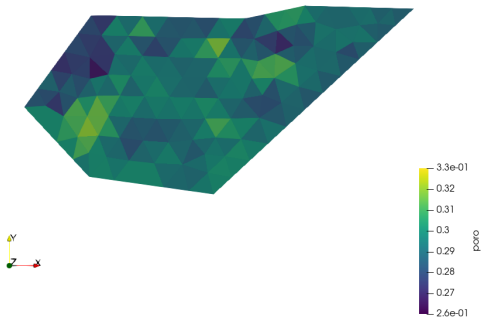

(b) Proxy porosity map

Figure 4.5: The original field and the proxy model porosity map for the Upper payzone.

4.2.3. Fluid and Rock Physics

The fluid model selected for the proxy model is DARTS dead oil model. Dead oil model means that the pressure must stay below the bubble point pressure and the fluid properties below this point will not consider int he fluid model of the simulation. In Dead oil model, there is no free gas released inside the reservoir, however, there might be free gas at the bottom hole of wells due to the pressure or rate control implemented on the well. As for the physical properties of the proxy rock, the Brooks-Corey correlation is used to evaluate the the relative permeability of the oil and the water. The prior knowledge of the rooks-Corey correlation parameters are taken straightly from the reference model with some small deviations to adjust the optimization settings.

4.2.4. Initial Condition

The initial static condition of the proxy model is set to be approximately equivalent to the reference model. despite the aquifer behavior and the distribution of the capillary pressure, all the other properties such as STOIIP, initial reservoir pressure at datum depth of 610m, well locations, average water saturation distribution and the average depth are approximately similar to that of reference model of the field.

4.2.5. Well Definition

In the unstructured grid mesh system, each well is located at the cell center and more than one well is not allowed to be perforated in a cell, therefore, a general methodology is required to translate the location of the wells and the perforations from the reference model to the proxy model. A python code

is developed to keep the spatial consistency between wells and organizing the completion of each well by taking the coordinate of the beginning and the end of the completion of each well. The coordinate of the completion is then translated as normalized coordinates to find the cell index of the unstructured grid cell. As for the evaluation of the *Well Indexes*, an equivalent circle inside each prism is assumed to develop the well index which can be a reasonable approximation of the true well index inside each unstructured grid cell. This modification is conducted based on the Peaceman model 2.27 described in section 2.4.2.

4.3. Data-driven DiWA Model

In this section, the DiWA model is examined with the realistic field data from an oil reservoir provided by industrial partner [2]. The configuration of this section is to first examine the simple DiWA model of the field and then detect outliers of the training results. The DiWA model is then modified step-by-step to investigate the improvement of the modification in each stage. Finally, the best strategy which reveals the most sensible outcomes will be evaluated evaluated. The properties and the field development strategies of the simple DiWA oil reservoir model are explained in details in section 4.1. Followed are some brief descriptions of the minor modifications of the DiWA model which are used to adopt the framework with the complexities of the oil reservoir. These modifications are:

- **Gross Liquid Rate Control**: Since the gross liquid rate of the wells from the field data is the most reliable values in hand, the framework, which was previously designed for BHP well control, have to be updated to handle the gross liquid rate control on each well.
- **Objective Function**: Regarding the changes in the well control strategies and the field reports about the reliability of the data, the objective function only considers the water production rate as the observed data and gross liquid rate as an input.
- **Multi-layer Initial Condition**: The oil reservoir encompasses two pay zones separated by an impermeable layer. The zones have different initial conditions both in terms of initial pressure and water saturation. Therefore, the framework is updated to handle multi-layer initial conditions.
- **Multi-layer Production**: In the segment of interest, there is one well stopping from producing from the upper zone and continue with only the lower zone. The model is updated with a feature to cover this modification.
- **Well Type Change**: In the segment of interest, there are two wells changing from producer to injectors at some points. Therefore, a copy injection well is added at the same location of the target producer and set to be activated at the time that the producer changes to injector.
- **Depletion to Flooding Transition**: Since the magnitude of the field production rate is significantly different in the depletion and the flooding period, the optimizer cannot train these two periods at the same time. Therefore, the depletion period is trained with a lower importance (weight) rather than the flooding period. In this strategy, the priors are first trained for the depletion period and then used as a pre-knowledge to generate new priors for the entire interval; thus, the objective function will be trained with different weights in the depletion and the flooding period.
- **Presence of Active Water Aquifer**: Since the field encompasses an active water aquifer, the proxy model must be able to handle the possible effect of the aquifer in the training procedure; thus, the model is updated for some of the wells in the lower layer to capture the effect of the aquifer.

4.4. Training of the Depletion Period

The way that the priors are selected is crucially important since the effect of the initial guess on the optimization performance is relatively significant. In the field model approach, the priors are created

[2] Shell Global Solutions International B.V.

using random sampling of the permeability and Corey parameters with the statistics similar to the field data. Since the porosity map of the oil field is assumed to be the most reliable petrophysical data, the proxy model's porosity map is created using geometric averaging method explained in section 4.2.2. As for the objective function, it is built based on the total water rate of the field and then the priors are filtered by water rate L2-norm misfit error.

4.4.1. Simple DiWA Model Training for the Depletion Period

There are three vertical wells active in the primary depletion of the reservoir namely; *PMM-92H1*, *PMM-205H1*, and *PMM-137H1* in which well 92H1 and 137H1 are completed in both upper and lower pay zones and well 205H1 is completed only in the upper layer. Figure 4.6 depicts the water rate and the total liquid rate of theses three wells. According to the figure 4.6, the water production of the well 92H1

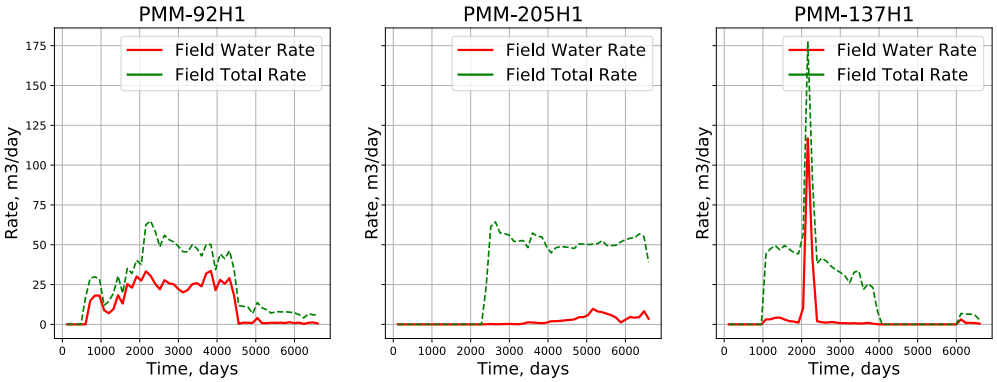

Figure 4.6: Water rate and total liquid production of the three wells producing during the depletion period.

is significantly higher than the other two wells and the water rate starts with a sharp peak in well 92H1. As for the well 137H1, one can easily observes a large water rate peak at time 2120 days which brought an inconsistency for the production history of the depletion period. As for the well 205H1, the water production is significantly lower than other two wells as this well is only completed in the upper pay zone.

For the very first attempt of training, the depletion period with no correction on well raw data is trained to investigate the optimizer responses specially for the high water production of the well 92H1 and the peak in well 137H1. Figure 4.7 illustrates the training results for theses three wells. The gray lines in the figure 4.7 are the priors which are fed to the optimizer and the blue lines represents the trained results.

4.4.2. Detecting Problems in the Depletion Period

As it is observed from the figure 4.7, the inconsistency of the priors in well 92H1 causes severe issues for the optimizer. All of the priors in this well are located below the true response which means that the model is not able to produce the desired amount of water and the optimizer is trying to increase the mobility of water in the entire reservoir. The issue inherent the high mobility of water is that the water production in the other wells (such as 205H1) becomes higher as a results of higher water mobility in the entire reservoir.

As for the well 205H1, the water rate starts with a very small magnitude at the starting point of the 2120 days. The model response could not capture this small value at the starting point. This issue can be as a result of wrong estimation oft he local water saturation or the initial non-linear parameters (i.e. Corey parameters) in the upper layer. If the optimizer train the non-linear parameters in a way that water becomes more mobile to satisfy the high production rate in well 92H1, the trained models for the well 205H1 will overestimate the water rate.

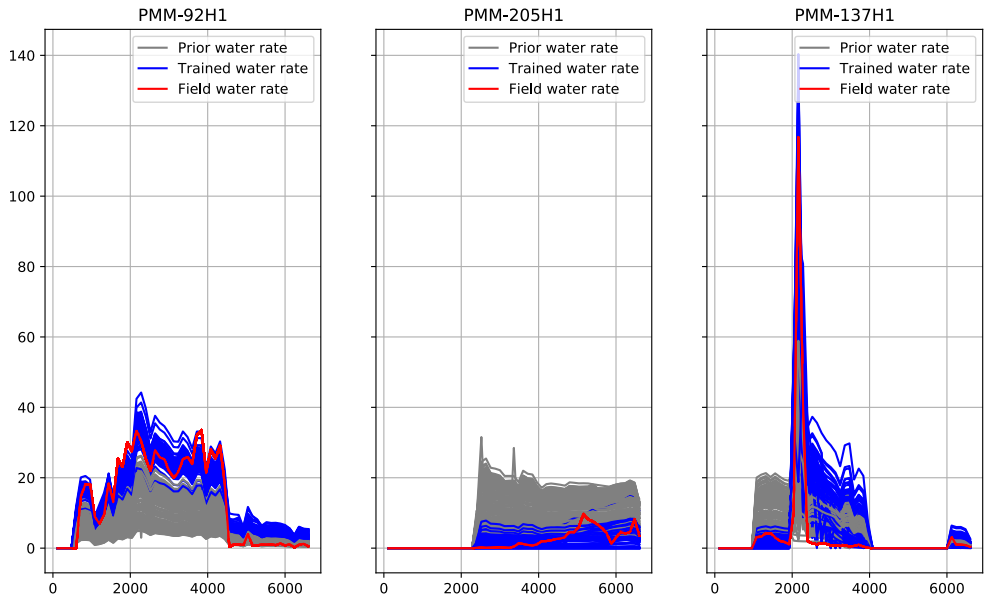

Figure 4.7: The training results for the depletion period. 200 priors (gray lines) are filtered in a way that water rate is relatively close to the true response. The blue lines represents the trained model response.

Investigating the water rate in the depletion period in each well, one can easily observe a large water rate peak in well 137H1 at time of 2120 days. This peak in the water rate is a consequence of partially abandoning of the upper zone in well PMM-137H1 from producing at time 1940 and continue to produce mainly from the lower zone. This change in the production strategy has led to a significantly large water rate peak in well PMM-137H1, which caused severe problems both in the prior generation and the training outcomes as it is clear in figure 4.7. This strange behaviour is not reasonable in this well and no acceptable explanation can be made to justify this behaviour.

4.4.3. Resolving Problems in the Depletion Period

The major correction in the strategy is that the non-linear parameters in the two layers must be trained separately, therefore, the Corey parameters region is extended from one to two regions; one for the upper layer and one for the lower layer. Well 92H1 is completed in the two layers and the lower layer is attached to an active water aquifer. The high water rate in the depletion period must be as a result of water leakage from a source out of the reservoir. As a result of this observation in well 92H1, an aquifer is added to the proxy model with a larger connectivity to the block which well 92H1 is completed. The aquifer must have a lower effect on other wells because, for instance, well 137H1 has no high water rate comparing to 92H1 and it is also completed at the both layers. The transmissibility between the aquifer and the lower layer is included in the training procedure, thus, the strength and the effect of the aquifer during the training is controlled by the optimizer.

Previously, the only petrophysical property that is mapped from the fine-scale to course-scale model was the porosity. Considering the new observations in the depletion period, specially the water production in well 205H1, the initial water saturation must be upscaled to the course-scale. To perform this upscaling, the local initial saturation at each well is detected and used for interpolating for other grid cells in the proxy model. Figure 4.8a depicts the original field initial saturation map for the upper layer and figure 4.8b represent the interpolated initial saturation map for the proxy model. By using this modification, the model is not initiating wells with overestimating water rate values.

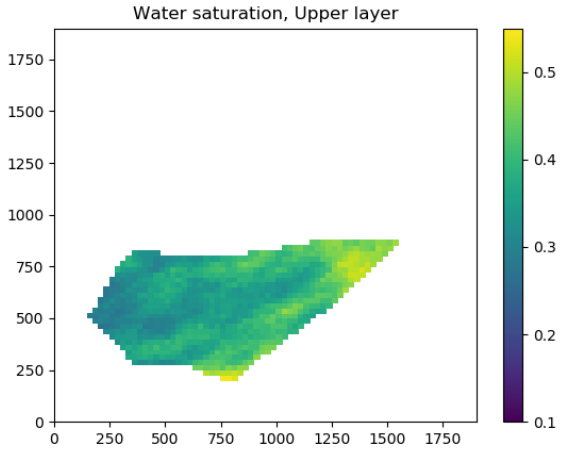

(a) The original field initial saturation map for the first layer.

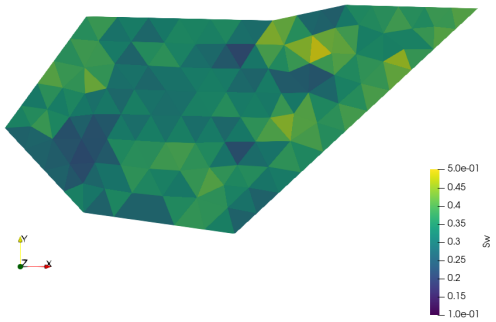

(b) The interpolated proxy model initial saturation map for the first layer.

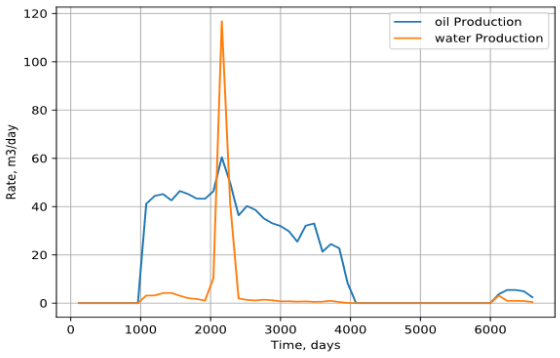

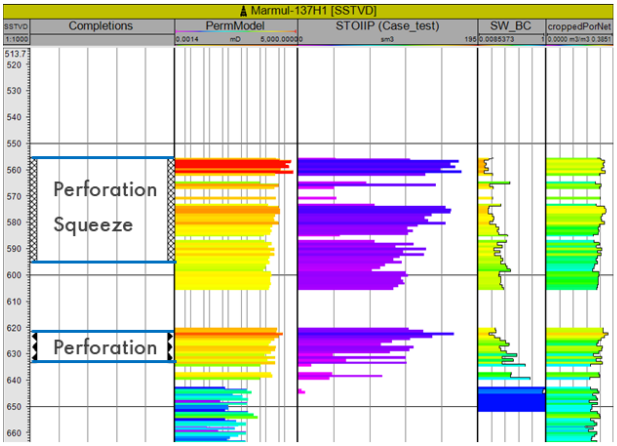

Figure 4.9: The well bore properties of the well *PMM-137H1* including: perforations, STOIIP, Initial water saturation, permeability and oil/water rate. The vertical axis is the SSTVD in meters. The water rate peak (the orange line peak in the left graph) occurred at the time of abandonment of the upper zone (SSTVD of 550 to 595) with squeeze cementing operation and continue to produce from the lower zone.

Figure 4.9 represents the perforations, wellbore properties and the water/oil rate production rates for the well 137H1. According to figure 4.9, the well is re-completed with a *squeeze cementing* operation which blocks the perforation in the upper layer and allows the liquid to be produced mainly from the lower zone. As it is clear from figure 4.9, the lower perforation is very close to the aquifer (the depth of the WOC can be interpreted from higher water saturation form the *Sw-BC* log) and this may cause the peak in the water rate. Comparing the peak with the previous timestep, this peak is significantly high (200 times larger than the previous timestep) and this is not logical. Another contributing reason inherent to the unexpected water rate peak would be that the time of the peak coincides the starting point of the well 205H1, which is only completed in the upper zone. There is no clear connection between wells 137H1 and 205H1 since the upper and the lower zones are separated from each other with an impermeable layer. As a result, it can be interpreted that the peak in water rate at well 137H1 is not normal and might be as a results of human or computational error. Figure 4.10 illustrates the training results for wells activated in the depletion period with new modifications explained above.

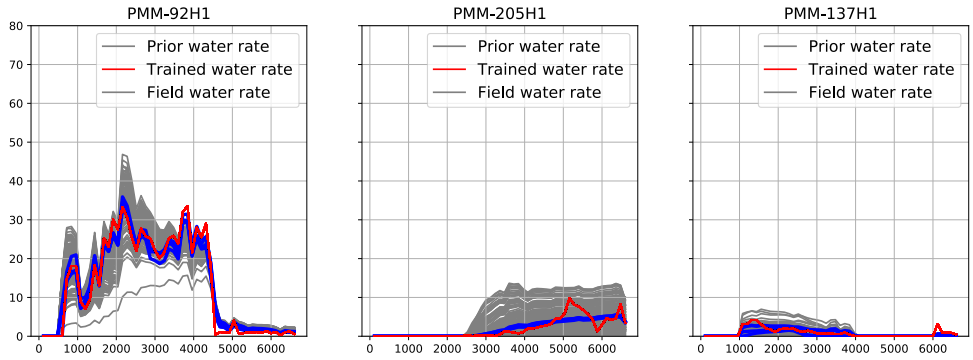

Figure 4.10: The training results for the depletion period with new modifications for resolving observed issues. 200 priors (gray lines) are filtered in a way that water rate is evenly distributed around the true response. The blue lines represents the trained model response.

As it is clear from the figure 4.10, the major issues in the training outcomes of the depletion period are resolved. The proxy model in well 92H1 produces evenly distributed priors with the support of the aquifer which has a higher transmissibility to the well block and could train the priors adequately with an acceptable misfit error (i.e. below 20 percent). Well 205H1 also starts with a reasonable small rate at the starting point and this was achieved because of the correction in local initial water saturation. Also the training results in the well137H1 did not crash and fluctuate because the large water rate peak in the data is removed from the observed inputs and the local water saturation is corrected. Figure 4.11 represents the total liquid rate, water rate and oil rate for the field data (red lines), priors (gray lines), and the trained models (blue lines). In the total gross liquid rate graph, there are only few outliers deviated from the true data and rest of the priors and the trained models are fitted with the field total gross liquid rate.

4.5. Training of the Flooding Period

In the flooding period, the source of water is not only the initial water in the reservoir, but the injectors will start to inject water. In order to train the flooding period, the priors must be selected from the trained models in the depletion period, however, the new priors might need some minor modifications and another filtering procedure. In addition to that, there are some wells locating in the boundary of the segment of interest and they might cause severe problems for the training process. In this section, the possible issues in the flooding period are discussed and some minor modifications are applied.

The priors for the flooding period is selected directly from the trained models in the depletion period for the first attempt. Figure 4.12 represents the trained model responses when running for the entire interval of the reservoir. As it is clear from the figure 4.12, the trained models for the depletion period

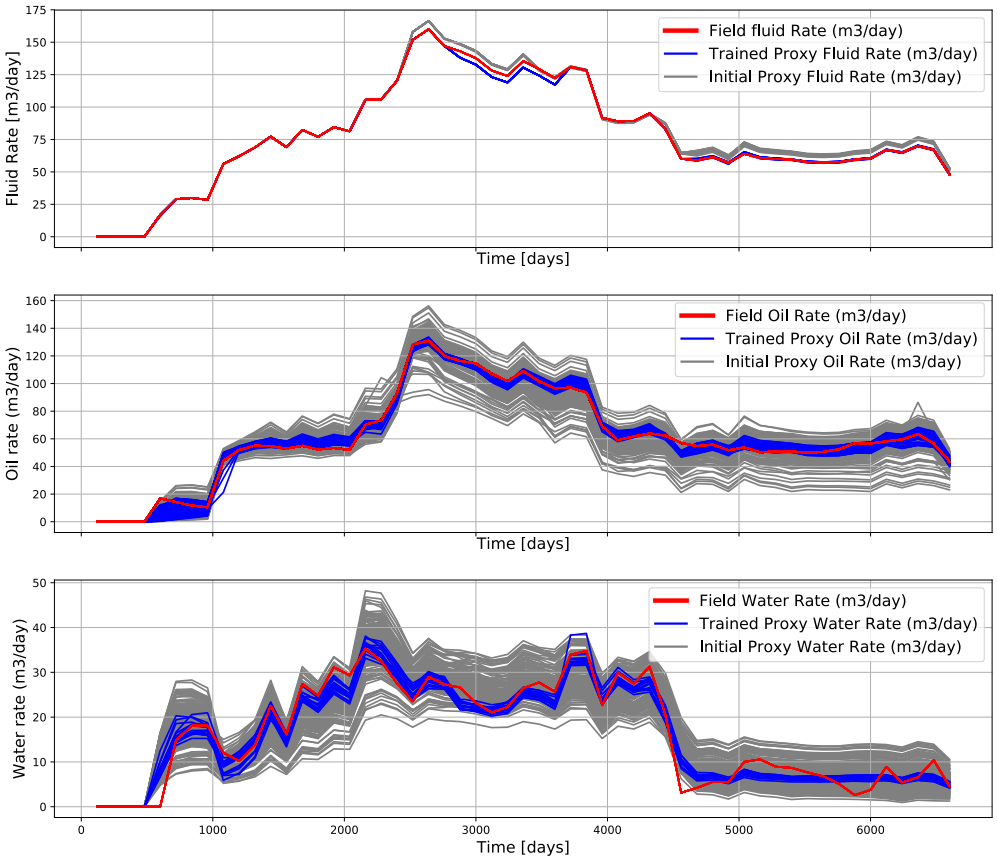

Figure 4.11: The total liquid rate, total water rate and total oil rate for the field data, priors and the trained models in the depletion period are depicted in this figure.

cannot predict adequately the flooding period. The trained parameters in the flooding period have made water less mobile than the oil and when the injection operation starts, the oil moves faster and is produced more than water. The alternative for selecting the priors for the entire reservoir lifetime

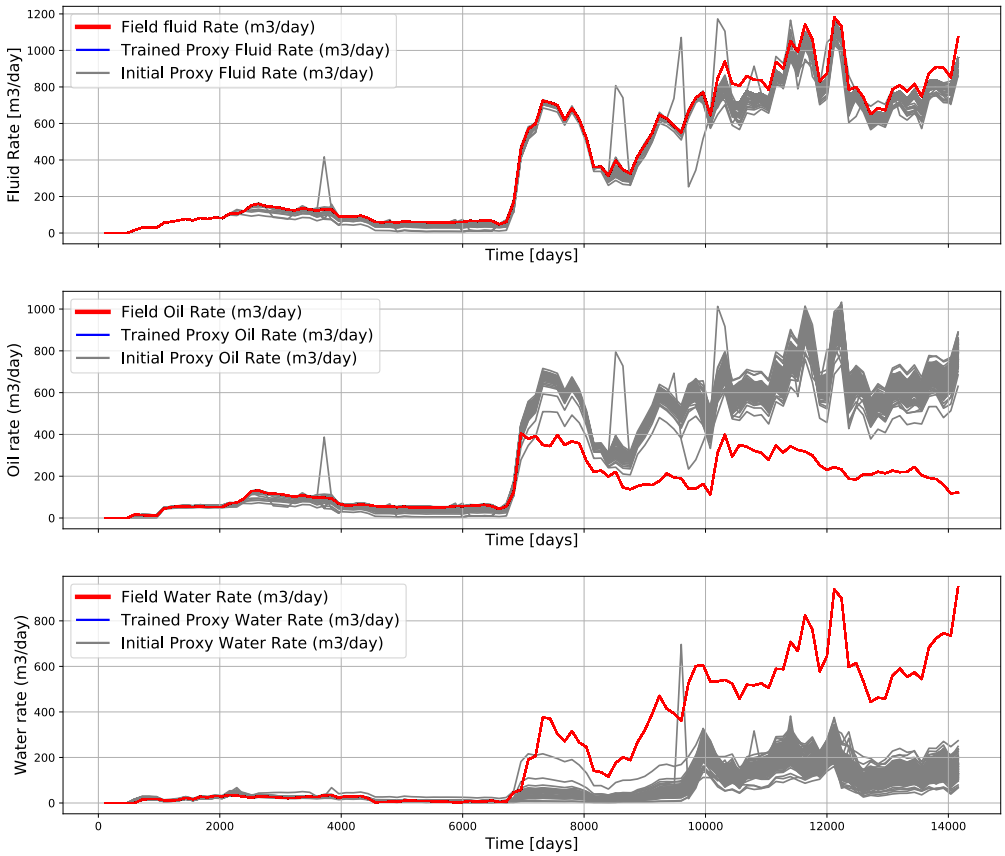

Figure 4.12: The total liquid rate, total water rate and total oil rate for the field data and the priors which are generated only based on trained models in the depletion period.

is to generate new priors for the whole interval by defining a new filtering procedure which covers both depletion and flooding. In the new filtering strategy, since the magnitude of the objective function is bigger than the depletion period, the depletion period gets larger weighting factor in the objective function than the flooding period. This strategy is also implemented in the training procedure. Figure 4.13 illustrates the new priors and the trained priors for the entire reservoir lifetime. From the total rate point of view, the trained models are fitted to the true data with a acceptable misfit error, however, there are some small parts with sever problems in total rates.

In order to investigate the details of the trained models, the oil rate for all if the wells must be demonstrated. Figure 4.14 depicts the training details for oil rate in each well with the new priors selection method described earlier. It is now clear that there are severe issues in the training outcome in most of the wells. An extra green line is added to the figures indicating the total rate of the well (water + oil) for better understanding of the each phase production separately. It is realized that the problematic wells are all located at the boundary of the model and some of the horizontal wells are completed partially inside the model and partially in the neighbouring segment. Now the assumption of sealing faults must be revised to take the effect of the boundary flows into the model. In such a case, these wells cannot

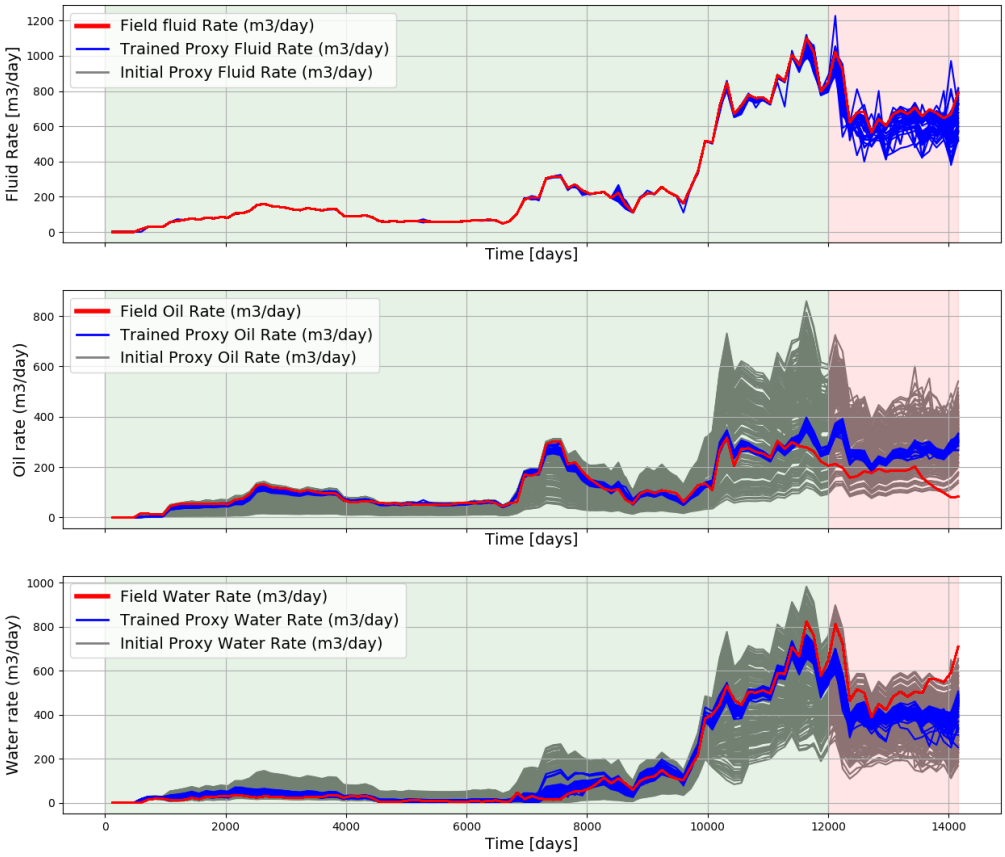

Figure 4.13: The total liquid rate, total water rate and total oil rate for the field data, priors and the trained models for the entire time interval of the reservoir with the new priors generated. The results contains all wells including wells completed near the boundary and partially inside the segment. Priors are trained with higher weight on objective function for the depletion period. The green and the red areas are the training and forecast intervals respectively.

be trained accurately in a data-driven framework. The possible solution is to first examine the interior well's (wells which are far from the boundary) performance in the current model (segment 2) when other boundary wells are excluded from the training. If the prior behaviour and the training performance of the interior wells become more consistent, the strategy of extending the boundaries can be applied.

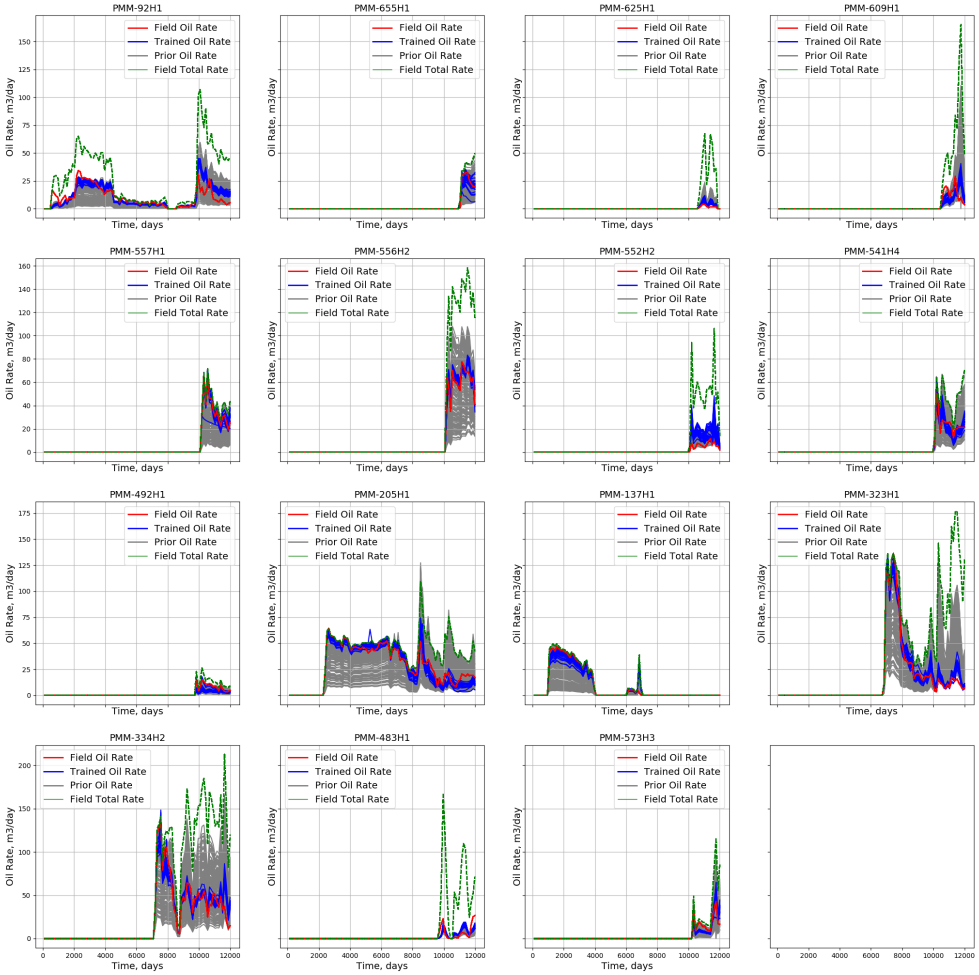

Figure 4.14: The total liquid and the oil rate for the field data, the priors, and the trained models for each well in the training interval (12000 days). The green line represents the total liquid rate for each well. The results contains all wells including wells completed near the boundary and partially inside the segment. Priors are trained with higher weight on objective function for the depletion period.

Figure 4.15 illustrates the training results for the interior wells excluding eleven boundary wells. As it is clear form the figure 4.15, the training performance was significantly improved and this indicates that the strategy in the current DiWA model, both in terms of prior selection and the training parameters, is reasonable. Therefore, the inconsistency in some of the results is a consequence of the flow from other segments. The assumption of sealing faults can be canceled with this observation and the effect of the boundary flow must be taken into consideration.

From the earlier mentioned outcomes, the effect of the boundary must be taken into account in the

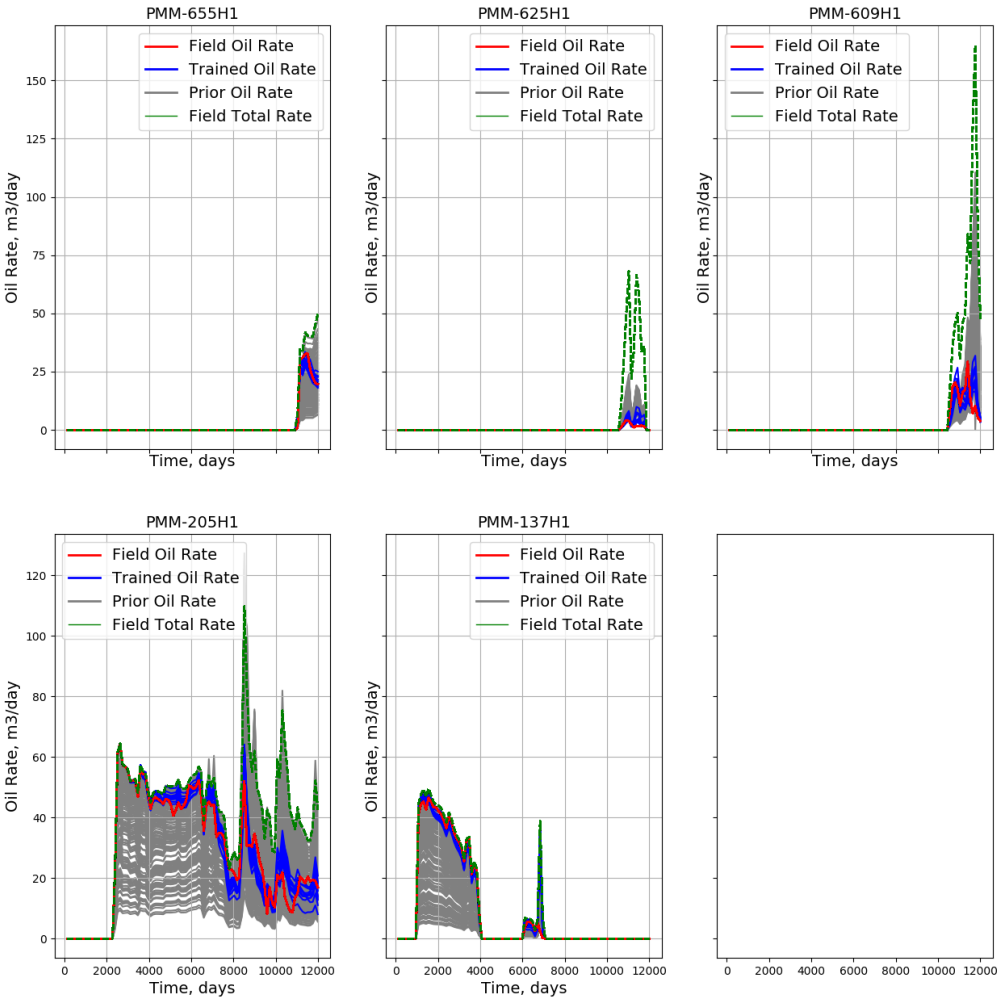

Figure 4.15: The total liquid and the oil rate for the field data, the priors, and the trained models for each interior well (wells which are far from the boundaries). The green line represents the total liquid rate for each well. Priors are trained with higher weight on objective function for the depletion period.

DiWA model. Therefore, further modifications have to be added to the DiWA model to cover the effect of the boundary and other segments:

- **Removing wells with lack of data**: There are three wells which are completed partially in the segment of interest and partially in the neighbouring segment. The field model doesn't have the data in these neighbouring regions, thus, these wells are removed form the training but they are actively performing in the model.
- **Boundary extension**: The boundaries of the model have to be constructed in a way that the model can capture the effect of the flows from the boundaries in addition to injectors and producers in the neighboring segments (see figure 4.16).

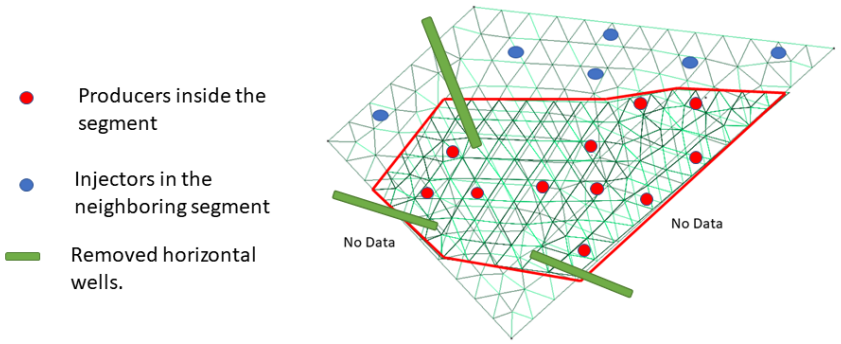

Figure 4.16: The extended version of the mesh to capture the effect of the neighboring segments and the boundary flows. Some boundaries have no available data to be added to the model. Blue circles are the approximate position of the new injectors added to the model.

Figure 4.17 depicts the final results of the field data-driven model for each individual wells. In these results, there are 12 producers participating in the training procedure and three wells in the segment 2 (323H1, 334H2, and 573H3) are removed from the training since there were no available data about neighbouring segment of these wells. The outcomes shown in the figure 4.17 are the best results for the DiWA model for this specific oil field in which the trained models of the priors are fitted within an average overall rate misfit of 10 percent. As mentioned previously, the overall misfit rate error is calculated using L-2 norm of the oil or water rate. Figure 4.18 also represents the prediction period (i.e., form 12000 to 14160 days) which indicates that the DiWA model is relatively able to predict the production history with quiet acceptable misfit error except for the later time (13800 to 14160 days). In this later time, there are two vertical wells converting from producer to injector, thus, the total water rate is underestimated by the proxy model. Converting a well from producer to injector has always been tricky to be resolved by the simulators, however, the DiWA model could capture the effect of this conversion to some extend.

In terms of total field oil and water production, figure 4.18 depicts an acceptable match of the true data with the trained model.As it is clear from figure 4.18, the total fluid rate of the production history, priors and the trained model are overlapping each other which means that the the well control of gross liquid rate is working accurately. The objective function is constructed based on the total water rate and the oil rate is simply evaluated form the trained water rate and the total gross liquid rate.

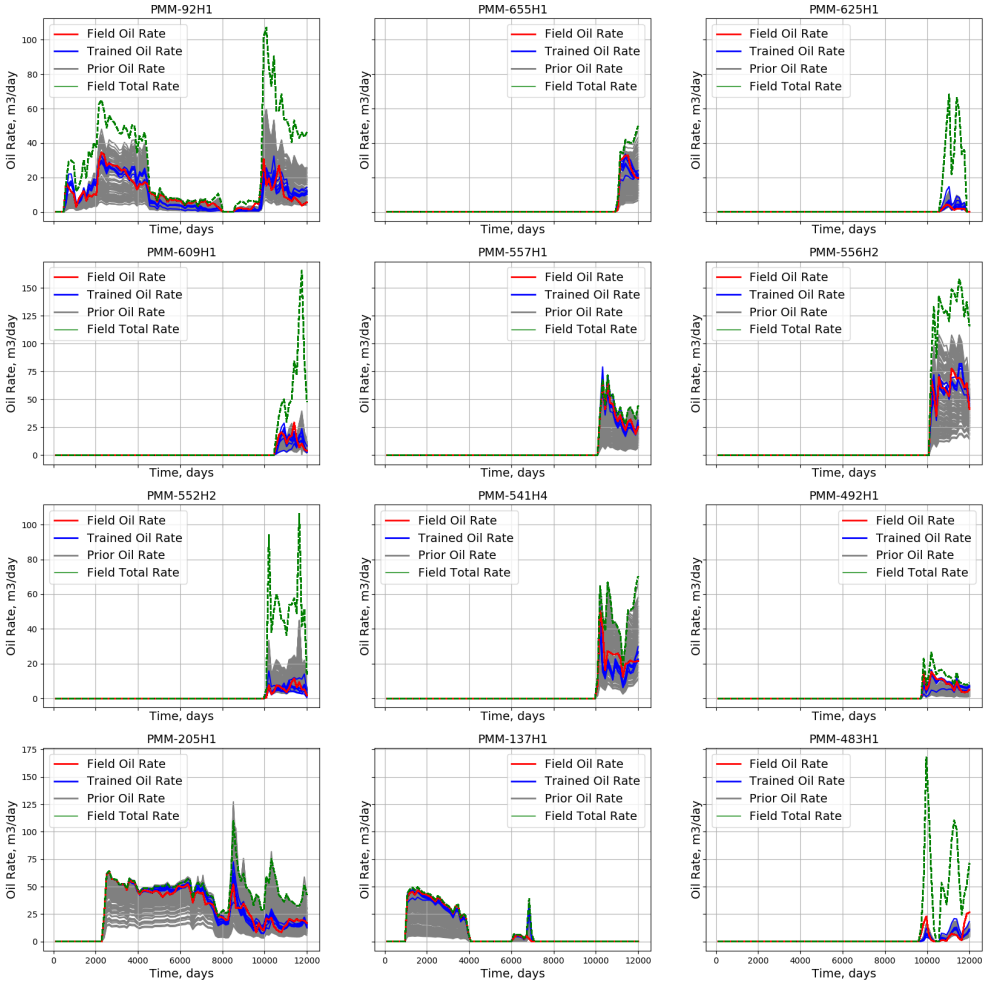

Figure 4.17: The total liquid and the oil rate for the field data, the priors, and the trained models for each well for the extended-boundary modification. The green line represents the total liquid rate for each well. Priors are trained with higher weight on objective function for the depletion period.

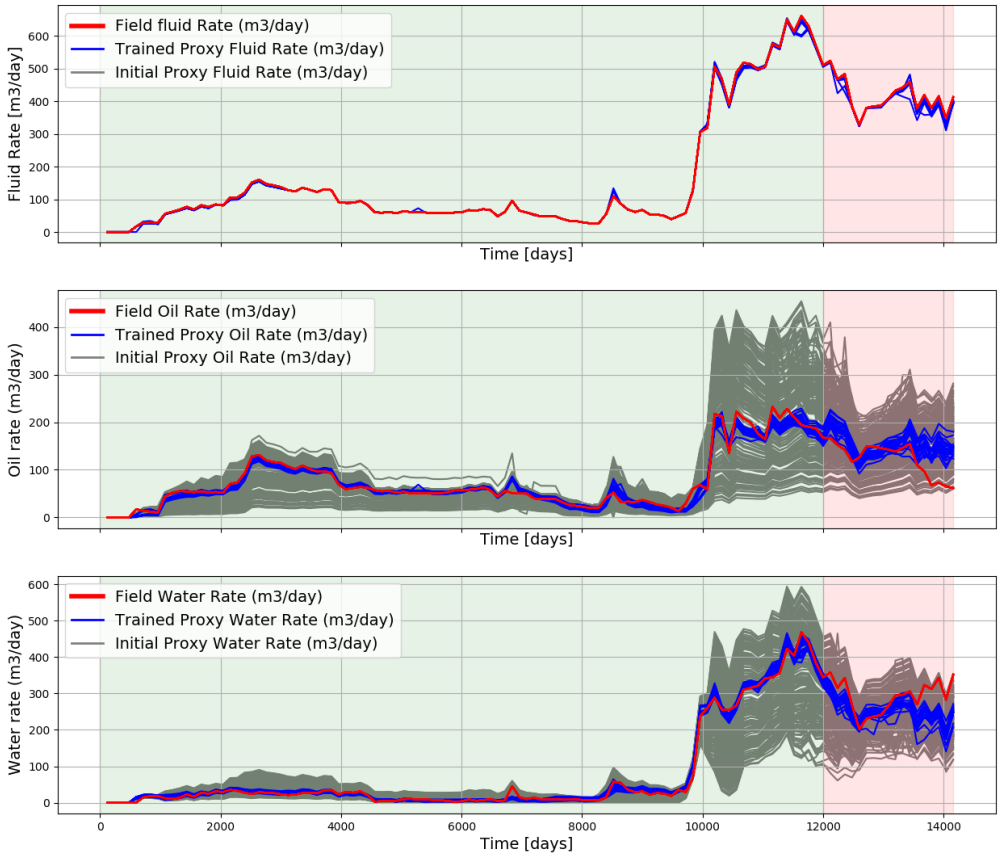

Figure 4.18: The total gross liquid rate, total water and total oil rate for the field data, the priors, and the trained models for the entire field for the extended-boundary modification excluding the three horizontal boundary wells. Priors are trained with higher weight on objective function for the depletion period. The green and the red areas are the training and forecast intervals respectively.

The main purpose of the proxy models are the ability of them to predict reservoir production in the future. The DiWA model is relatively successful predicting the oil history after the training time of 12000 days. There is one significant issue observed in the forecast period which is the lower water production rate compared to the field data. This problem may caused by the well type change from producer to injector at 13160 days which is outside the training period. At this time, well 92H1, which is located at the boundary of segment (see figure 4.19) and completed in two pay zones, changes to injector and consequently the field water production increases. The increase in water production reveals that the injecting water at this time is not contributing to the oil production. On the other side, the water rate in the proxy model decreases in this period, which is different from the field behaviour. This mismatch behaviour between the proxy model and the filed might be because of the flow from the boundaries or specific connections between the upper and the lower pay zones.

In order to diagnose the issues in each wells and the relationship between their mismatch error and their location in the segment, figure 4.19 is generated. According to figure 4.19, wells 552H2 and 541H4, which don't have neighbouring cells even in the extended boundary version, have relatively higher errors. Well 92H1 is completed in two layers and has a stronger connectivity to the aquifer among other wells. Even when the extended-boundary strategy is applied, well 92H1 is not improving as the other wells and this indicates that this well may have other issues that is not considered in this framework. There are plenty of uncertainties in this model which leads to inconsistency in some wells such as tilted layers (specially in the aquifer), ignoring capillary and the gravity effect, faults transmissibilities, and errors in the the raw data. The effect of the uncertainties in a field scale approach will result in severe issues in the DiWA framework, however, the final training results are relatively consistent and could resolve the uncertainties. Perhaps the most important learning from this project would be the effect of the boundary flows on the DiWA model. This was the first trial of the data-driven framework on a reservoir with active boundary flows and complex well connectivity.

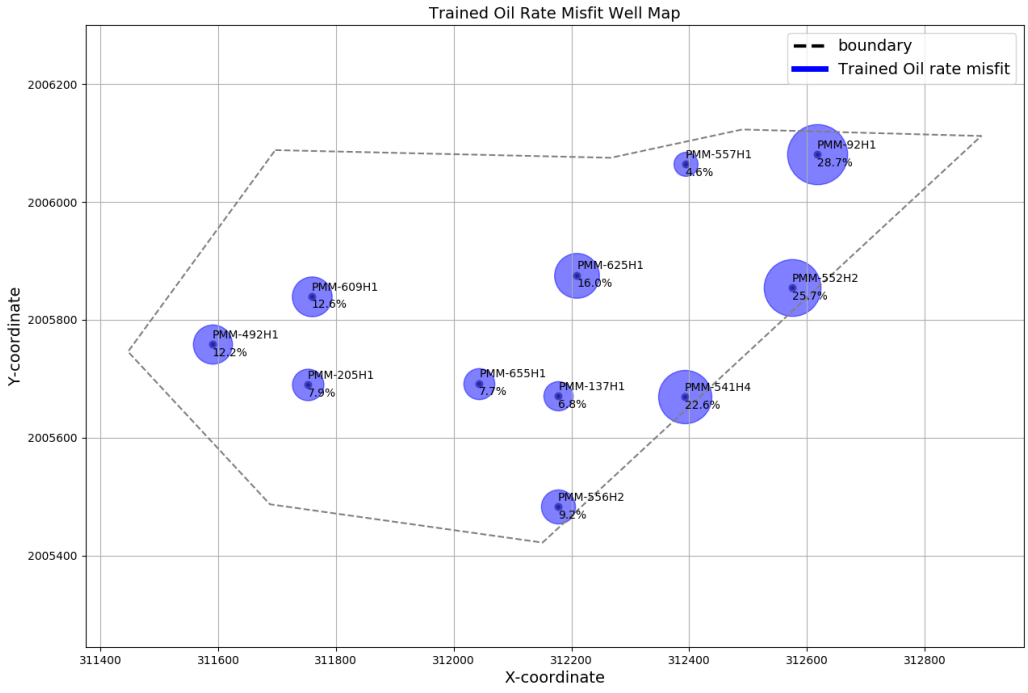

Figure 4.19: The oil rate mismatch error for each vertical wells and their locations in segment 2.

5

Future Work

The DiWA is a powerful methodology that is able to train complex data-driven reservoir model only with simple knowledge of the geological properties and general structure of the reservoir. It is shown in this research that some parameters have significant influences on the training which are not taken into account. It would be beneficial to add other extra modifiers to the training parameters of the optimizer such as reservoir initial water saturation and injection water rate. since the water saturation is normally modeled with resistivity logs, the reliability of this data is relatively high and it would be more effective to estimate the initial water saturation with more precise upscaling techniques and include it in the training procedure. As for the injectors, depending on the reliability of the field reports, the injection rate can be trained within a realistic range in the model to improve the effect of injection in the flooding period. Another enhancement that can be considered in the DiWA framework is to capture the boundary effect before running the optimization. The flows from transmissible faults and boundaries can cause sever problems to the training results and make the optimizer to estimate the training parameters within unrealistic ranges.

6

Conclusion

In this research, the newly developed DiWA methodology is examined for the optimization performance and the reliability of results using various priors built from the well information. Additionally, the DiWA model was validated by realistic field data, and some improvements and modifications were applied to the framework.

As for the optimization performance, it is shown that the influence of the geological priors is significant in terms of rate mismatch error and iteration. A closer prior model to the reference reservoir response will lead to more accurate training results with lower optimization iteration; however, a close prior is not essentially converged to the true model parameters due to the ill-posedness of the problem. In principle, the DiWA model is capable to reconstruct the reference reservoir parameters in a stochastic approach for prior ensemble of models. In the proposed methodology, the priors are filtered to be close to the true response and are generated from the exact statistics of the reference model. However, it can not be assured that the DiWA model can reconstruct the reference reservoir parameters (i.e., permeability) for all prior models since the solution to the history matching problem is not unique.

In the realistic field model, a few points must be highlighted as a learning outcome of this project. First, the quality of the production and the BHP data significantly impact optimization performance and must be checked in advance. The failure of optimizer to converge to true response often indicate an inconsistency between the model assumptions and reality. For example, in the training at the depletion period for the realistic field, an abnormal behaviour in the production history for one of the well at certain period was detected. After farther investigation, the abnormal historical behavior was explained by work-over operations which have not been accounted in the model. For simplicity, it was decided to correct the well data and eliminate the discontinuity in the production history.

Second, the driving mechanisms in the reservoir, such as an active aquifer, can influence the data-driven model to a large extend, especially in the depletion period, in which the source of extra water in the reservoir is from the aquifer. In the oil field in our study, only one well experiences high water production in the depletion period which can only be explained by the presence of an active aquifer. Therefore, our initial assumption on inactivity of aquifer was not supported and the aquifer has been added to the proxy model. In addition to driving mechanisms, the estimation of the initial water saturation for the proxy model can significantly affect the training results, especially at each producer's starting time in the depletion period. To consider this fact, the initial water saturation distribution based on log interpretation was introduced to the proxy model.

Third, the flow from the boundaries is crucially important in the data-driven model when applied to a segment of the entire model since the changing condition at the boundary will create fluid inflow and alter the amount of fluid initially estimated inside the proxy model (i.e., STOIIP). It has been shown that the wells located near the segment boundary could not be trained as efficiently as other wells.

Extending the reservoir boundaries and adding wells from the neighbouring segment could resolve this issue efficiently; however, the boundary flow always exists and will cause the mismatch in well's history located at the boundary.

In conclusion, to achieve a consistent proxy model for a realistic reservoir, constant petrophysical parameters such as porosity and local water saturation must be evaluated from logs or other field information. Besides, there might be numerous inconsistencies in historic data which reflects the development strategy implemented in the field, such as changing downhole completion or work-over operations. In such cases, the failure of optimizer to converge to the historic data can identify potential inconsistencies and require their corrections through either adjustment of historic data or model parameters. Regarding the boundary effect, the proxy model should benefit the flexibility to capture the effect of boundary flows, especially on wells near the boundaries, to reveal consistent training results for the entire reservoir lifetime.

Bibliography

[1] Jørg E. Aarnes, Vegard Kippe, and Knut-Andreas Lie. “Mixed multiscale finite elements and streamline methods for reservoir simulation of large geomodels”. In: *Advances in Water Resources* 28.3 (2005), pp. 257–271. ISSN: 0309-1708. DOI: https://doi.org/10.1016/j.advwatres.2004.10.007. URL: https://www.sciencedirect.com/science/article/pii/S0309170804001885.

[2] Alejandro Albertoni and Larry W. Lake. “Inferring Interwell Connectivity Only From Well-Rate Fluctuations in Waterfloods”. In: *SPE Reservoir Evaluation and Engineering* 6.01 (Feb. 2003), pp. 6–16. ISSN: 1094-6470. DOI: 10.2118/83381-PA. eprint: https://onepetro.org/REE/article-pdf/6/01/6/2135655/spe-83381-pa.pdf. URL: https://doi.org/10.2118/83381-PA.

[3] A.C. Antoulas. “Approximation of Large-Scale Dynamical Systems: An Overview”. In: *IFAC Proceedings Volumes* 37.11 (2004). 10th IFAC/IFORS/IMACS/IFIP Symposium on Large Scale Systems 2004: Theory and Applications, Osaka, Japan, 26-28 July, 2004, pp. 19–28. ISSN: 1474-6670. DOI: https://doi.org/10.1016/S1474-6670(17)31584-7. URL: https://www.sciencedirect.com/science/article/pii/S1474667017315847.

[4] A Brooks R. Cprey. “Hydraulic properties of porous media”. In: *hydrology papers* 3 (1964).

[5] Vladislav Bukshtynov et al. “Comprehensive framework for gradient-based optimization in closed-loop reservoir management”. In: *Computational Geosciences* 19.4 (Aug. 2015), pp. 877–897. ISSN: 1573-1499. DOI: 10.1007/s10596-015-9496-5. URL: https://doi.org/10.1007/s10596-015-9496-5.

[6] M. A. Cardoso, L. J. Durlofsky, and P. Sarma. “Development and application of reduced-order modeling procedures for subsurface flow simulation”. In: *International Journal for Numerical Methods in Engineering* 77.9 (2009), pp. 1322–1350. DOI: https://doi.org/10.1002/nme.2453. eprint: https://onlinelibrary.wiley.com/doi/pdf/10.1002/nme.2453. URL: https://onlinelibrary.wiley.com/doi/abs/10.1002/nme.2453.

[7] Anindya Chatterjee. “An introduction to the proper orthogonal decomposition”. In: *Current Science* 78.7 (2000), pp. 808–817. ISSN: 00113891. URL: http://www.jstor.org/stable/24103957.

[8] Jean-François Remacle Christophe Geuzaine. *A three-dimensional finite element mesh generator with built-in pre- and post-processing facilities*. 2009. URL: https://gmsh.info/.

[9] Mark Khait Denis Voskov. *Delft Advanced Terra Simulator*. 2013. URL: https://darts.citg.tudelft.nl/.

[10] Christophe Geuzaine and Jean-François Remacle. “Gmsh: A 3-D finite element mesh generator with built-in pre- and post-processing facilities”. In: *International Journal for Numerical Methods in Engineering* 79.11 (2009), pp. 1309–1331. DOI: https://doi.org/10.1002/nme.2579. eprint: https://onlinelibrary.wiley.com/doi/pdf/10.1002/nme.2579. URL: https://onlinelibrary.wiley.com/doi/abs/10.1002/nme.2579.

[11] Allan Haldane. *NumPy; numerical computation*. 2005. URL: https://numpy.org/.

[12] C. He and L.J. Durlofsky. “Structured flow-based gridding and upscaling for modeling subsurface flow”. In: *Advances in Water Resources* 29.12 (2006), pp. 1876–1892. ISSN: 0309-1708. DOI: https://doi.org/10.1016/j.advwatres.2005.12.012. URL: https://www.sciencedirect.com/science/article/pii/S0309170806000145.

[13] Thomas Y. Hou and Xiao-Hui Wu. “A Multiscale Finite Element Method for Elliptic Problems in Composite Materials and Porous Media”. In: *Journal of Computational Physics* 134.1 (1997), pp. 169–189. ISSN: 0021-9991. DOI: https://doi.org/10.1006/jcph.1997.5682. URL: https://www.sciencedirect.com/science/article/pii/S0021999197956825.

[14] *Non-Stationary Estimation of Reservoir Properties Using Production Data*. Vol. All Days. SPE Annual Technical Conference and Exhibition. SPE-38729-MS. Oct. 1997. DOI: 10.2118/38729-MS. eprint: https://onepetro.org/SPEATCE/proceedings-pdf/97SPE/All-97SPE/SPE-38729-MS/1941807/spe-38729-ms.pdf. URL: https://doi.org/10.2118/38729-MS.

[15] J.D. Jansen. “Adjoint-based optimization of multi-phase flow through porous media – A review”. In: *Computers and Fluids* 46.1 (2011). 10th ICFD Conference Series on Numerical Methods for Fluid Dynamics (ICFD 2010), pp. 40–51. ISSN: 0045-7930. DOI: https://doi.org/10.1016/j.compfluid.2010.09.039. URL: https://www.sciencedirect.com/science/article/pii/S0045793010002677.

[16] P Jenny, S.H Lee, and H.A Tchelepi. “Multi-scale finite-volume method for elliptic problems in subsurface flow simulation”. In: *Journal of Computational Physics* 187.1 (2003), pp. 47–67. ISSN: 0021-9991. DOI: https://doi.org/10.1016/S0021-9991(03)00075-5. URL: https://www.sciencedirect.com/science/article/pii/S0021999103000755.

[17] M. Karimi-Fard, L. J. Durlofsky, and K. Aziz. “An Efficient Discrete-Fracture Model Applicable for General-Purpose Reservoir Simulators”. In: *SPE Journal* 9.02 (Apr. 2004), pp. 227–236. ISSN: 1086-055X. DOI: 10.2118/88812-PA. URL: https://doi.org/10.2118/88812-PA.

[18] M. Karimi-Fard, L. J. Durlofsky, and K. Aziz. “An Efficient Discrete-Fracture Model Applicable for General-Purpose Reservoir Simulators”. In: *SPE Journal* 9.02 (Jan. 2004), pp. 227–236. ISSN: 1086-055X. DOI: 10.2118/88812-PA. URL: https://doi.org/10.2118/88812-PA.

[19] Los Alamos National Laboratory Kitware Inc. *Large Data Visualization*. 2005. URL: https://www.paraview.org/overview/.

[20] Wes McKinney. “Data Structures for Statistical Computing in Python”. In: *Proceedings of the 9th Python in Science Conference*. Ed. by Stéfan van der Walt and Jarrod Millman. 2010, pp. 56–61. DOI: 10.25080/Majora-92bf1922-00a.

[21] R. E. Mortensen. “Stochastic Optimal Control: Theory and Application (Robert F. Stengel)”. English. In: *SIAM Review* 31.1 (Mar. 1989). Copyright - [Copyright] © 1989 © Society for Industrial and Applied Mathematics, pp. 153–2. ISSN: 00361445. URL: https://www.proquest.com/scholarly-journals/stochastic-optimal-control-theory-application/docview/926139685/se-2?accountid=27026.

[22] Dean S. Oliver and Yan Chen. “Recent progress on reservoir history matching: a review”. In: *Computational Geosciences* 15.1 (Jan. 2011), pp. 185–221. ISSN: 1573-1499. DOI: 10.1007/s10596-010-9194-2. URL: https://doi.org/10.1007/s10596-010-9194-2.

[23] D. W. Peaceman. “Interpretation of Well-Block Pressures in Numerical Reservoir Simulation With Nonsquare Grid Blocks and Anisotropic Permeability”. In: *Society of Petroleum Engineers Journal* 23.03 (May 1983), pp. 531–543. ISSN: 0197-7520. DOI: 10.2118/10528-PA. URL: https://doi.org/10.2118/10528-PA.

[24] Schlumberger. *Exploration and Production Software*. 2005. URL: https://www.software.slb.com/products/petrel.

[25] X. Tian et al. “Discrete Well Affinity Data-Driven Proxy Model for Production Forecast”. In: *SPE Journal* 26.04 (Aug. 2021), pp. 1876–1892. ISSN: 1086-055X. DOI: 10.2118/205489-PA. eprint: https://onepetro.org/SJ/article-pdf/26/04/1876/2475398/spe-205489-pa.pdf. URL: https://doi.org/10.2118/205489-PA.

[26] Pauli Virtanen et al. “SciPy 1.0: Fundamental Algorithms for Scientific Computing in Python”. In: *Nature Methods* 17 (2020), pp. 261–272. DOI: 10.1038/s41592-019-0686-2.

[27] Denis V. Voskov. “Operator-based linearization approach for modeling of multiphase multi-component flow in porous media”. In: *Journal of Computational Physics* 337 (2017), pp. 275–288. ISSN: 0021-9991. DOI: https://doi.org/10.1016/j.jcp.2017.02.041. URL: https://www.sciencedirect.com/science/article/pii/S0021999117301444.

[28] Ali A. Yousef et al. “A Capacitance Model To Infer Interwell Connectivity From Production and Injection Rate Fluctuations”. In: *SPE Reservoir Evaluation and Engineering* 9.06 (Dec. 2006), pp. 630–646. ISSN: 1094-6470. DOI: 10.2118/95322-PA. eprint: https://onepetro.org/REE/article-pdf/9/06/630/2136093/spe-95322-pa.pdf. URL: https://doi.org/10.2118/95322-PA.

[29] *INSIM: A Data-Driven Model for History Matching and Prediction for Waterflooding Monitoring and Management with a Field Application*. Vol. Day 2 Tue, February 24, 2015. SPE Reservoir Simulation Conference. D021S007R004. Feb. 2015. DOI: SPE-173213-MS. eprint: https://onepetro.org/spersc/proceedings-pdf/15RSS/2-15RSS/D021S007R004/1465035/spe-173213-ms.pdf. URL: https://doi.org/SPE-173213-MS.

Appendix A: Trained Parameters

In the original filed model, only one Corey correlation is used for the entire reservoir; however, in the DiWA model, there are two various Corey regions to be trained by the optimizer to capture the effect of higher water saturation and connectivity to the aquifer in the lower layer. It was previously mentioned that the trained parameters are the reservoir transmissibilities, well indexes, and the Corey parameters. Therefore, discussing the resulted trained parameters of the best strategy of the DiWA model is of a great importance. Figure A.1 illustrates the trained Corey parameters; *Corey exponents*, *residual saturation*, and *end point mobility* for the upper and the lower layer (there are two Corey regions to be trained in the DiWA model). As it is clear from the scatter plot in figure A.1 that the behaviour of fluid in the upper and the lower layer is set to be different in terms of water fluid mobility. A.1a, A.1b, and A.1c According to the theory, the relative permeability of a super course proxy model such as the current DiWA model, is different from the field data, therefore, for better understating of this concept, the relative permeability of the trained and the real model [1] for averaged values of the results are plotted together and shown on figure A.2. It can be interpreted from the figure A.2 that the trained Corey model is relatively more water-wet than the field Corey model which means that the optimizer has made the water less mobile than oil in the entire reservoir to match the observed data.

[1] Real model relative permeability means the data from the laboratory.

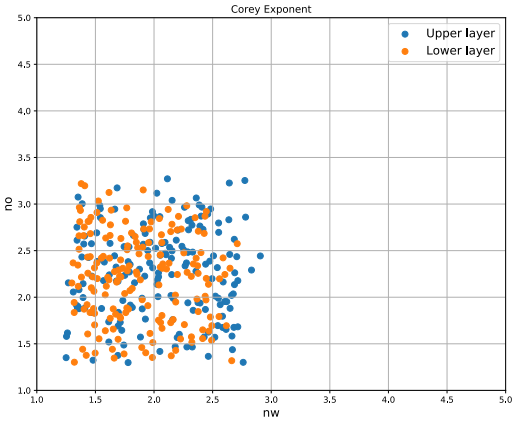

(a) Trained Corey exponent

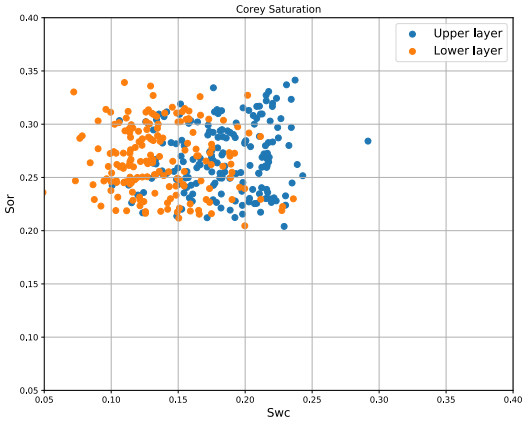

(b) Trained Corey Saturation

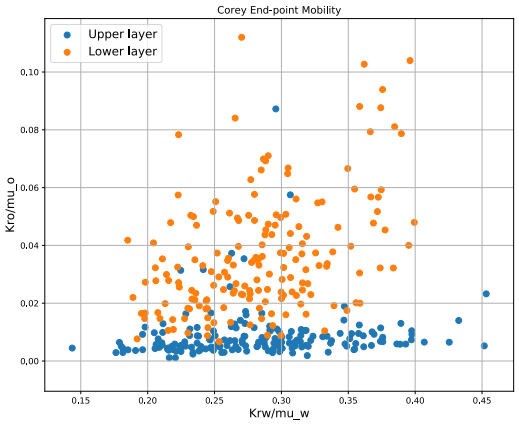

(c) Trained Corey end point mobility

Figure A.1: Trained Corey parameters for the boundary-extensions strategy.

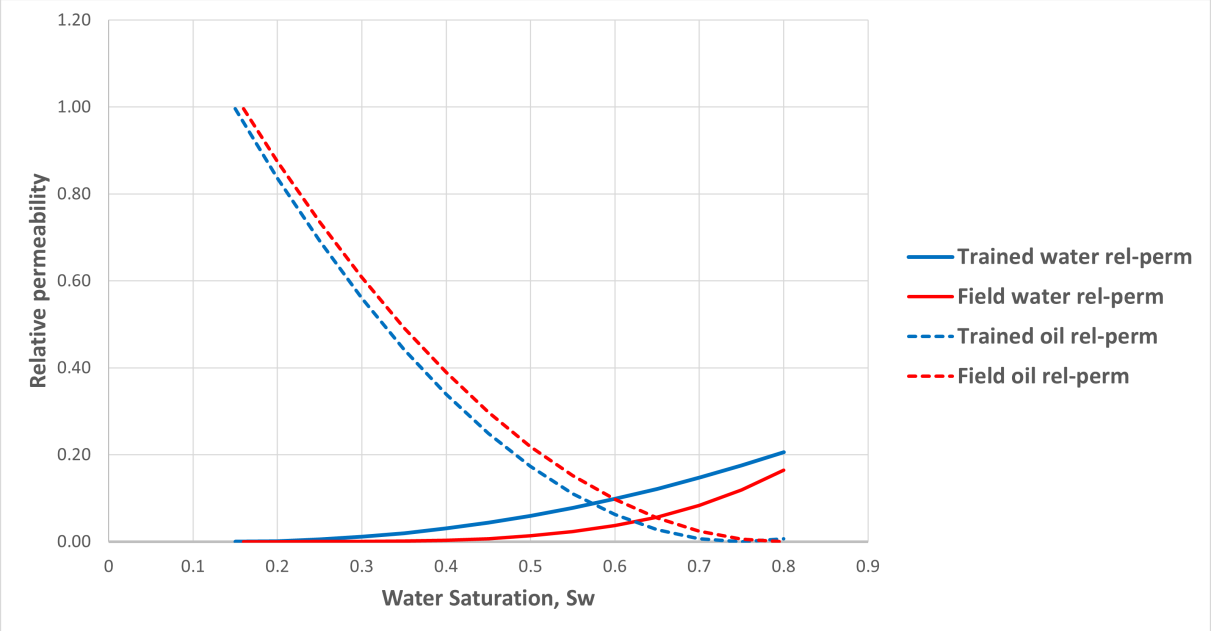

Figure A.2: The relative permeability curves for the field (lab) data and the trained models. The average value of the trained parameters are used to evaluated trained relative permeability curves.